remote sensing

MDPI

Article

A Fully Automated SETSM Framework for Improving the Quality of GCP-Free DSMs Generated from Multiple PlanetScope Stereo Pairs

Myoung-Jong Noh [1,*] and Ian M. Howat [1,2]

[1] Byrd Polar and Climate Research Center, The Ohio State University, Columbus, OH 43016, USA; howat.4@osu.edu
[2] School of Earth Sciences, The Ohio State University, Columbus, OH 43016, USA
* Correspondence: noh.56@osu.edu

Highlights

What are the main findings?

- Automatic SETSM framework for PlanetScope PS2 DSM generation;
- Improvement of DSM quality with optimized stereo pair selection and inter-plane vertical coregistration.

What are the implications of the main findings?

- Optimized stereo pair selection with sequential filtering process and weighted stereo pair index effectively and automatically identifies well-defined stereo pairs.
- Inter-plane vertical coregistration improves both DSM quality and consistency and reduces vertical errors by up to 43% in RMSE without existing reference surfaces.

Abstract

We investigate the potential of frequent repeat imagery acquired by the PlanetScope Dove small satellite constellation to overcome temporal and spatial limitations in automated surface topography mapping. While individual PlanetScope Dove stereo pairs produce low-quality Digital Surface Models (DSMs) with large height uncertainties, the high temporal frequency enables multiple DSMs to enhance accuracy through multiple-pair image matching. We present a fully automated SETSM framework by improving the quality of PlanetScope Dove DSMs based on SETSM Multi-Pair Matching Procedure (SETSM MMP). This framework enhances stereo pair quality through an optimized stereo pair selection by sequential conditional filtering and a Weighted Stereo Pair Index (WSPI). A novel inter-plane vertical coregistration, which minimizes scaling errors between single stereo pair DSMs, was developed to improve consistency and accuracy in DSM quality without reference surfaces. Applied to the cloud-obscured Pantasma crater region in Nicaragua, the optimized stereo pair selection automatically selects well-defined stereo pairs. The inter-plane vertical coregistration without existing reference surfaces achieves up to a 43% Root Mean Square Error (RMSE) reduction and 26% improvement in distribution within a 5 m vertical error. DSM quality correlated strongly with tile size, stereo pair convergence angle, asymmetric angle and terrain-dependent scale variability. The proposed framework provides fully automatic, high quality PlanetScope Dove DSMs without Ground Control Points (GCPs).

Keywords: multiple-pair; PlanetScope; DSM; SETSM; image matching

Check for updates

Academic Editor: Akira Iwasaki

Received: 9 January 2026
Revised: 27 February 2026
Accepted: 2 March 2026
Published: 6 March 2026

Copyright: © 2026 by the authors. Licensee MDPI, Basel, Switzerland. This article is an open access article distributed under the terms and conditions of the Creative Commons Attribution (CC BY) license.

1. Introduction

Stereo-photogrammetric DSM generation from optical imagery is highly sensitive to image quality and viewing geometry. Atmospheric conditions such as clouds and fog directly affect surface visibility and the extent of recoverable surface topography in stereo pair imagery (i.e., stereo pairs). The image feature matching process relies on image radiometric quality to correctly locate corresponding features through comparison of image textures. Image viewing geometry determines ground sample distance (GSD), surface occlusions, and convergence angle between stereo pairs, all of which determine the achievable DSM accuracy and quality through the image-matching process. Conventional satellite imaging platforms, such as MAXAR's WorldView constellation, offer stereo-mode, submeter-resolution image acquisition optimized for high-quality DSM generation. These stereo pairs have convergence angles greater than 30°, GSD finer than 0.5 m, and high radiometric quality, resulting in DSMs of decimeter precision and consistent quality from single stereo pairs. However, spatial and temporal coverage of this imagery is limited by atmospheric conditions, revisit frequency, and cost. To expand satellite coverage at low costs, but with a loss in DSM quality, large numbers of repeat, lower radiometric quality and resolution imagery obtained from SmallSats may be used. Currently, Planet Inc. operates a constellation of more than 100 PlanetScope 3U CubeSats with a coverage of 300 million+ km^2 a day (https://www.planet.com/products/satellite-imagery-of-earth/, accessed on 26 December 2025) [1]. The PlanetScope CubeSats use a frame sensor and include three instruments: PS2 (Dove Classic), PS2.SD (Dove-R), and PSB.SD (SuperDove) (https://docs.planet.com/data/imagery/planetscope/techspec/, accessed on 16 February 2026) [2]. These instruments provide orbit direction and satellite geometry information, including azimuth, viewing and incidence angles, along with latitude and longitude coordinates in geodetic WGS84 coordinates for image acquisition parameters. In addition, PlanetScope imagery is offered in two geometric formats of basic and ortho. Compared to the PS2.SD and PSB.SD, which create multiple-band composite images from band-stripe frame images acquired with different projection centers and viewing angles, the PS2 provides original frame images for visible and NIR bands with a single projection center, with a 3.0 m to 4.2 m GSD and a limited, off-nadir looking angle of up to ±5°. Therefore, PS2 images can be utilized to compose stereo pairs for DSM generation by avoiding the composition errors caused by multiple projection center locations and viewing angle differences in band-stripe frame images.

PlanetScope multiple-band images with frequent acquisitions and extensive spatial coverage have been widely utilized to monitor land use and land cover change, as well as Earth system processes and hazards ([3–9]). The satellite configurations are intended for surface monitoring rather than production of stereo-photogrammetric DSMs. Individual stereo pairs have a maximum 10° convergence angle, which results in larger height uncertainty and less consistent, and generally lower, quality than DSMs from conventional, i.e., WorldView, stereo-mode stereo pairs with convergence angles greater than 30°. To improve the stereo pair DSM quality, a single, high-quality DSM may be generated by combining multi-pair DSMs of lower quality from the large number of repeat images over short periods of time (days). Cloud-free PlanetScope PS2 images were utilized to generate DSMs with 5 m posting over three regions: Mount Teide in the Canary Islands of Spain, Nanga Parbat massif in the western Himalaya, and Khurdopin glacier in the Shimshal valley of the Karakoram [10]. More than 50 stereo pairs with a minimum B/H ratio of 1:60 were applied in DSM generation, with heights obtained from the median value of semi-global matching (SGM, [11]) between pairwise DSMs. The vertical accuracy of DSMs for Mount Teide and Nanga Parbat was 4 to 5 m over stable terrain, compared with 5 m from airborne LiDAR and 30 m from DSMs created from ALOS imagery. For the Khurdopin

glacier, only six images from two overpasses with B/H ratios of 1:13 were to generate a DSM with a reduced height accuracy of 9 m due to low redundancy for height estimation. PlanetScope PS2 DSMs at 9 m postings were used to measure elevation changes over the Shisper glacier in the Hunza valley of the Karakoram, using 16 and 14 cloud-free images from two separate years [12]. Comparing these DSMs to 30 m resolution Shuttle Radar Topography Mission (SRTM) and 2 m resolution stereophotogrammetric DSMs created from WorldView-2 and GeoEye-1 imagery yielded validation accuracies of 12 m and 7 m, respectively. A PlanetScope PS2 DSM was generated from 100 stereo pairs with convergence angles of greater than 6°, with height values obtained from the median of pairwise semi-global DSMs over forested regions in Catalonia, Spain, resulting in a 5.5 m height accuracy compared to airborne LiDAR [13]. Three criteria were considered for selecting PlanetScope images for DSM generation over mountainous, forested, and urban regions: (1) a cloud cover of 0%, (2) 100% coverage of the target area, and (3) avoidance of temporally varying surfaces such as snow or water [14]. To improve DSM quality, stereo pairs with convergence angles mostly greater than 8° were selected in DSM processing. A hierarchical SGM algorithm was applied to generate pairwise DSMs, and a fused DSM was produced with a weighted median filtering method [15]. The resulting PlanetScope DSM with a 4 m posting has a vertical accuracy of 4 to 6 m compared with a LiDAR DSM, which is sufficient to detect large vertical surface changes, such as landslides. Thus, multiple-pair PlanetScope DSMs may provide time series of surface topography at global scales with high temporal resolution and wide spatial coverage, providing an up to 4 m vertical accuracy depending on the number and quality of images, image viewing geometry and surface type.

To minimize blunders and outliers in DSMs, previous studies manually selected only cloud-free images. Cloudy images, however, provide partially visible areas and can provide additional pairs with well-defined viewing geometry, improving DSM quality by increasing the number of height estimates. Typical applications select only those stereo pairs that fully overlap a defined area of interest (AOI) boundary to minimize vertical bias with GCPs and reference surfaces, avoiding relative coregistration errors between partially overlapping DSMs. However, this approach potentially excludes high-quality stereo pairs with partial coverage and limits DSM generation to AOI's that are comparable to the image footprint size. To utilize stereo pairs that partially cover the target AOI, a method is required for automatically minimizing coregistration errors. This is achieved by adjusting relative height uncertainties between partially overlapping DSMs resulting from variability in terrain and viewing geometry, without ground control points (GCPs) or reference surfaces. The accuracy of DSMs created in previous studies mostly relies on manually determined stereo pair configurations, which are defined by the number and selection of images under predefined criteria. In addition, prior approaches apply domain-specific criteria to identify favorable stereo viewing geometries over limited local areas. These manual and case-dependent procedures are therefore not suitable for the automated generation of high-quality, spatially consistent PlanetScope PS2 DSMs over larger areas from massive volumes of repeat imagery.

Here, we aim to improve the quality of large-scale PlanetScope PS2 DSMs with an automated DSM generation framework based on the SETSM Multiple-Pair Matching Procedure (SETSM MMP, [16]), which applies a 3D kernel-based weighted height estimation (KWHE) that accounts for stereo pair geometry and utilizes the Surface Extraction from TIN based Search-space Minimization (SETSM) algorithm. The SETSM software package (version 4.3.16) is open-source, HPC-optimized, and fully automated, requiring no terrain-specific parameters and manual intervention. SETSM only requires image orientation information such as Rational Polynomial Coefficients (RPCs) and camera parameters. The fully automated SETSM framework, designed for single conventional satellite stereo pairs with

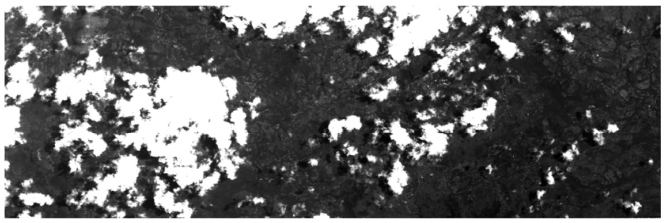
well-defined viewing geometry, has extensively demonstrated robust performance and produced consistent, high-quality DSMs in the ArcticDEM and REMA continental-scale terrain mapping projects as described in [16]. Building upon this prior development, we propose new methodologies for both automatic stereo pair configuration and height error minimization in merged DSMs based on a relationship between DSM quality and the viewing geometry of PlanetScope PS2 single stereo pairs. These are required to enable a fully automated high-quality PlanetScope PS2 DSM generation. We therefore develop a sequential conditional filtering method and Weighted Stereo Pair Index (WSPI) to automatically identify optimal images, select well-defined stereo pairs among PlanetScope PS2 images, and optimize computational efficiency. This algorithm incorporates stereo pair geometry and cloud and tile coverage to optimize the number of stereo pairs and improve DSM quality when using partially overlapping stereo pairs. We utilize previously determined relationships between DSM accuracy/quality and stereo pair geometry [17] in an automated stereo pair selection scheme. Further, we develop an inter-plane vertical coregistration method specialized for PlanetScope PS2 single DSMs that automatically generates reference surfaces by improving DSM quality and consistency, aligning pairwise height surfaces and minimizing vertical bias among relative single DSMs. This method addresses large height uncertainties caused by narrow stereo pair convergence angles and is particularly effective for partially overlapping DSMs.

We first describe an overall framework for automatically generating PlanetScope PS2 DSMs over arbitrarily sized areas in Section 2. Section 3 explains novel methodologies for improving the quality of PlanetScope PS2 DSMs generated from the framework. An automated sequential stereo pair selection methodology utilizing the WSPI is presented. To remove blunders and offsets, we develop a sequential, inter-plane vertical coregistration method that minimizes vertical biases between partially overlapping DSMs using geometric and scaling error analysis, without GCPs or a reference DSM. In addition, we present a modified 3D KWHE in which the weighting terms are replaced with estimates derived from the inter-plane vertical coregistration step. A tile mosaicking method is described to construct seamless, large-scale DSMs by adjusting relative vertical biases between tiles over edge buffer areas. In Section 4, we test the framework with PlanetScope PS2 imagery over a highly clouded area in the Pantasma crater and analyze accuracy and quality of tiled DSMs with USGS SRTM DSM and a WorldView stereo pair DSM in terms of viewing geometry and terrain surface variability. In addition, four other craters (Oasis and British Petroleum Structure crater in Libya, Bigach crater in Kazakhstan, and Iturralde crater in Bolivia) are tested to generate DSMs. We discuss the experimental results and summarize our study in Sections 5 and 6.

2. Automatic SETSM Framework for PlanetScope PS2 DSM Generation

Our main goal is to provide an automatic SETSM framework for generating high-quality, large-scale DSMs from available PlanetScope PS2 imagery without manual filtering of low-quality images impacted by partial cloud cover and radiometric saturation, as shown in Figure 1. Obtaining multiple image stereo pairs over the same regions is essential to improve the quality of DSMs from PlanetScope PS2 images by minimizing height uncertainties arising from their narrow, off-nadir looking geometry. In addition, combinations of various stereo-viewing geometries, such as convergence angle, asymmetry angle (AA), and bisector elevation angle (BEA), as well as an appropriate image-matching strategy, are crucial to improve the quality and accuracy of PlanetScope multiple-image-derived DSMs (PSMDSM). The asymmetry angle, AA, is the angle between a bisector and a line perpendicular to the baseline of a stereo pair, and the bisector elevation angle (BEA) is the elevation angle of a bisector of the convergence angle and indicates the obliqueness of the

epipolar line [18]. The height accuracy of stereo-photogrammetric DSMs improves with geometrically well-defined stereo pairs involving large convergence and bisector elevation angles and small asymmetry angles. Since cloud-free pixels in partially clouded images with wide off-nadir looking angle can configure well-defined stereo pairs and provide valuable texture information in stereo image matching, our DSM generation framework does not simply filter out the images based on cloud coverage information in the provided ephemeris data as in past applications ([10,12–14]). Instead, we include all useful imagery to increase the possible number of stereo pairs with small enough temporal baselines (i.e., the acquisition time interval between two images) that changes in the surface between images are minimized. Although cloudy and saturated pixels cause blunders and outliers on single DSMs, the proposed framework excludes those errors through an iterative procedure to obtain accurate heights from multiple single DSMs described and validated in Section 4.



(a) Partially cloudy image (34% cloud coverage)



(b) Partially radiometrically saturated image

Figure 1. Examples of low-quality PlanetScope PS2 images. (**a**) An image with 34% cloud coverage and (**b**) an image with radiometric saturation.

Figure 2 describes an overall framework for the automatic DSM generation from PlanetScope PS2 imagery based on SETSM algorithm. Planet Inc. has application programming interfaces (APIs) for discovering imagery and ordering bundles of imagery and analytic products (https://docs.planet.com/develop/apis/, accessed on 26 December 2025) [19]. Based on a defined target boundary and temporal baseline of a few months, available PlanetScope PS2 images from the Planet APIs are transferred into a database in a computing system. The temporal baseline is a flexible parameter that depends on the surface stability of the target region over time and directly influences image-matching quality, which is determined by image texture. Depending on the specifications of the specific computing system, the target boundary is divided into tiles for processing, with sizes that optimize computational loads. Starting from the first tile, candidate images in the database are initially selected according to user-defined starting and ending dates for image acquisition time (a temporal baseline for DSMs), an overlapped ratio with the tile area, and cloud coverage, which are accessible in the ephemeris data. The quality and accuracy of stereo-photogrammetric DSMs generated from stereo pairs with convergence angles less than 10 degrees are much more sensitive to viewing geometry than conventional satellite stereo-mode pairs with convergence angles greater than 30 degrees. The dependence of DSM accuracy and quality on stereo pair geometries, including convergence angles, the difference in azimuth angles, the GSD difference between two images, and the RPC biases are analyzed for the case of a narrow convergence angle [17]. Based on those results, we develop an optimized, fully automated, stereo pair selection scheme that utilizes a novel

Weighted Stereo Pair Index (WSPI). From the initial set of stereo pairs, one optimal height at each Matching Point (MP) on the DSM is estimated by an adaptation of the SETSM Multi-Pair Matching Procedure (SETSM MMP), whose performance has been validated by comparing SGM [16]. Based on SETSM MMP, weighted optimal heights are estimated through the 3D kernel-based weighted height estimation (3D KWHE) method by modifying the optimal height weights with estimates derived for PlanetScope PS2 stereo pairs, after adjusting relative vertical biases between optimal heights extracted from each stereo pair through the developed GCP-free inter-plane vertical coregistration algorithm. By iteratively updating 3D surfaces from the weighted optimal heights, RPC errors in each stereo pair can be relatively compensated for to improve single stereo pair DSM quality without GCPs [20]. The vertical coregistration can be skipped if (1) one reference image, which is the left image for all left-right stereo pairs, is available that covers the entire tile area; (2) the overlapping area of stereo pairs configured with the reference image covers the entire tile area; and (3) the stereo pairs with the reference image are sufficient to accurately estimate the optimal heights on the same reference image object-plane. However, this ideal condition is limited by image availability and tile size. Most cases involve partial coverage of the reference image and partial overlap of the tile area due to a lack of various stereo-viewing geometries to minimize the height uncertainty. To enable automatic, generalized DSM generation covering the entire tile area, all available stereo pairs are used in this framework, regardless of the availability of the single reference image. Relative RPC biases for each stereo pair are independently compensated on different reference object-planes, and vertical coregistration is applied to remove relative vertical biases between the bias-free optimal heights from stereo pairs. The final, weighted optimal heights are then estimated from the vertically co-registered, optimal heights of each stereo pair. After processing at the coarsest pyramid level, the availability of stereo pairs is updated based on the matching results. This iterative process continues until all tiles are completed. To provide large-scale DSMs, all tiles with buffers are mosaicked by adjusting relative vertical biases within a buffer area of overlap between tiles.

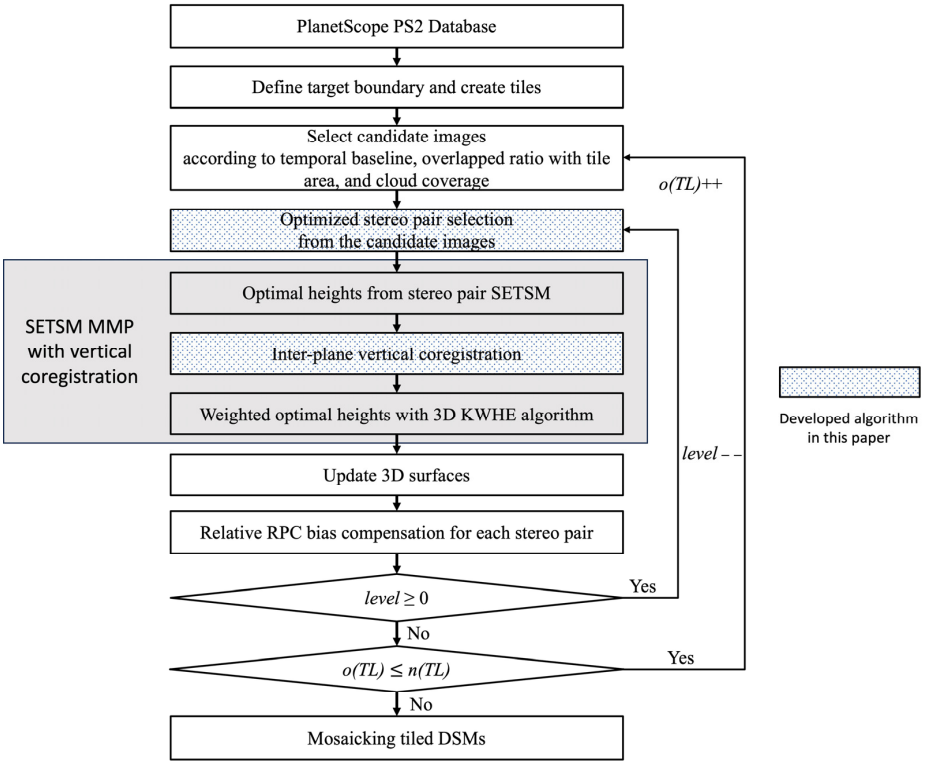


Figure 2. SETSM framework for automated PlanetScope DSM generation. *o(TL)* and *n(TL)* are the order of tiles and the total number of tiles, respectively. *level* is the pyramid processing level.

3. Detailed Methodology

This section presents the four main methodologies based on the automated SETSM framework, including two novel and two adapted methods. The two novel methods are (1) optimized stereo pair selection from the candidate images that fills the tile area to eliminate voids in the DSM and preferentially selects geometrically well-defined stereo pairs to improve overall DSM quality, and (2) GCP-free, inter-plane vertical coregistration to minimize relative vertical biases between single stereo pair DSMs (or heights) whose RPC biases are relatively compensated for in the stereo pair. The two adapted methods are (3) the optimal height estimation from multiple stereo pair optimal heights by applying the 3D KWHE in SETSM MMP through a modification of the weighting scheme and (4) mosaicking of DSM tiles to produce a single, seamless DSM over an area of any size.

3.1. Optimized Stereo Pair Selection

A novel optimized stereo pair selection procedure evaluates four factors to automatically select the best stereo pairs among the image database: (1) computing system capabilities (i.e., available cores and memory) to prevent processing failures by limiting a maximum number of stereo pairs, nSP_{max}; (2) tile coverage by stereo pairs to prevent voids; (3) consistency of DSM quality by defining a minimum number of stereo pairs for each MP, nSP_{min}; and (4) priority of stereo pairs depending on viewing geometries, cloud coverage, and tile overlap to improve DSM quality. To achieve automated DSM generation from a large number of images over diverse terrains, robustness and reliability of the processing framework is the fundamental requirement to ensure failure-free operation. To accurately estimate the required computing resources to apply SETSM, it is essential to analyze the SETSM methodology in terms of its computational demands. SETSM utilizes a geometrically constrained blunder detection algorithm based on 3D triangulated irregular network (TIN) structures that provides spatial proximity between features and estimates optimal heights by reducing possible outliers and blunders. Notably, SETSM uses the global distribution of all the matched point properties within the tile area to minimize the search space, geometrically remove blunders, and extract optimal heights, while not using locally divided sub-sampled areas to individually estimate the optimal heights at each MP. Thus, the entire area of the stereo pair images overlapping the tile are allocated to physical memory and are accessed for processing at each coarse-to-fine pyramid level. Besides the memory allocated for the input imagery, SETSM requires a much larger amount of physical memory for 3D voxel information that includes matching attributes and results for each stereo pair. This memory usage increases as a power of 2 with each successive coarse-to-fine pyramid level. To prevent memory allocation and access problems while processing at finer pyramid levels, nSP_{max} and tile size are limited based on the specifications of the computing system. On a system with a physical memory of 150 GB and SETSM memory usage, we set nSP_{max} to 100 and the tile size to 10 km by 10 km. A minimum number of repeat stereo pairs, $nSP_{min,}$ was also defined to ensure adequate tile coverage and consistent DSM quality, which is highly sensitive to the number of available stereo pairs and configuration of viewing geometries. Based on the analysis in [17], an nSP_{min} of 10 was used for automated processing. Subsequently, the nSP_{min} could be adaptively reduced to a new minimum value of 3 according to the convergence angle distribution and the total number of selected stereo pairs. Since the number of optimal heights (or matched heights) extracted from the selected stereo pairs at each MP was not determined before executing the matching process, a list of the selected stereo pairs was iteratively updated during pyramid-level processing by developed sequential filtering and adding processes, which were designed to preferentially select stereo pairs with less cloud coverage, wider CA and larger tile coverage. This iterative process increases the possibility of selecting

high-quality stereo pairs by removing low-quality stereo pairs and enhances DSM quality by including lists of stereo pairs in nSP_{min}. Based on the matching results at each pyramid level, low-quality stereo pairs from the previous level were filtered out for the next level of processing. The remaining stereo pairs were then ranked according to priority, which was determined by a developed Weighted Stereo Pair Index (WSPI), to efficiently reduce the total number of stereo pairs in nSP_{max} while improving DSM quality.

3.1.1. Initial Stereo Pair Selection

Figure 3 describes the initial stereo pair selection starting with the defined nSP_{max} and nSP_{min} at the first pyramid level. The number of initial stereo pairs, SP_{init}, is limited to two times the value of nSP_{max} to prevent exceeding the system's physical memory and to avoid over-filtering for high-quality stereo pairs. The list of SP_{init} is then reduced and optimized by counting the number of stereo pairs at each MP limited by nSP_{min}.

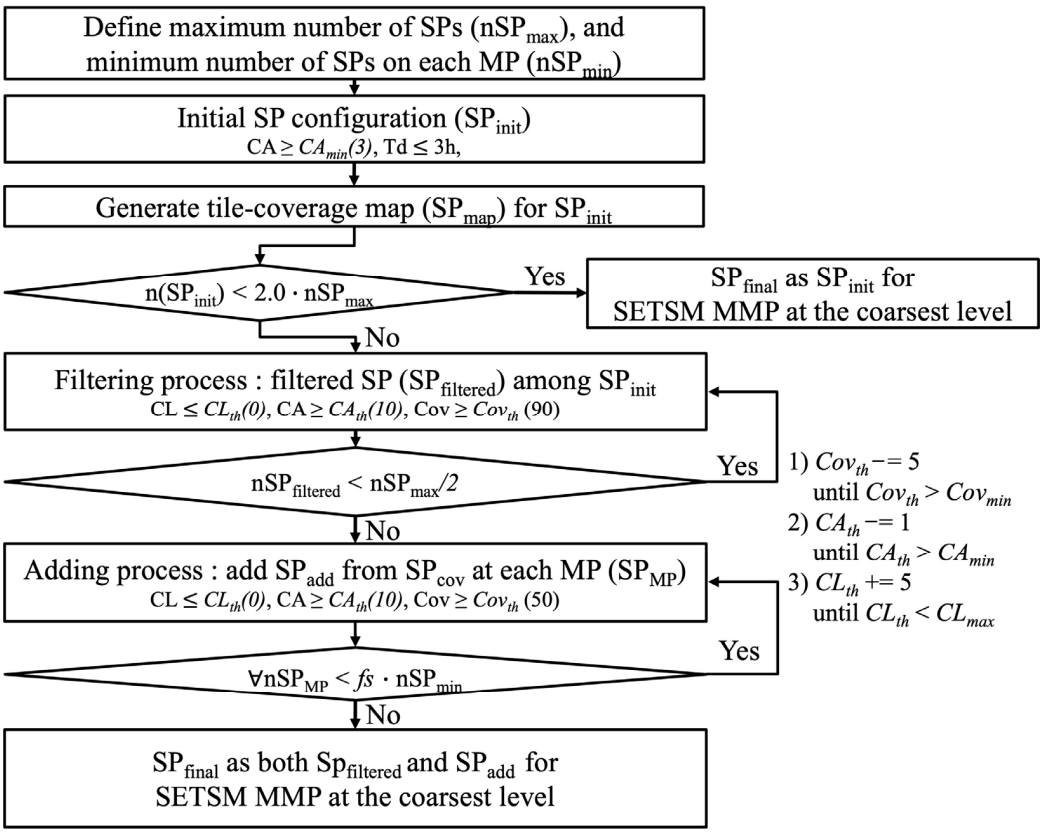


Figure 3. Diagram of the initial stereo pair selection for the first-pyramid-level processing through developed sequential filtering and adding processes.

The stereo pairs configured from the candidate images, all of which must satisfy the initial conditions of maximum temporal baseline, minimum tile overlap (Cov_{min}) of 30% and maximum cloud coverage (CL_{max}) of 50%, are iteratively selected by optimizing four parameters: convergence angle (CA), two texture conditions of cloud coverage (CL), image acquisition time difference (Td), and tile overlap (Cov). These represent one geometric parameter, two image texture parameters and one mapping parameter, respectively. CL_{max} ensures that a minimum required number of images are selected in persistently clouded areas, and images including more clouds than CL_{max} are mostly filtered out in our experiments. The CA is crucial for determining parallax between corresponding points and, consequently, height and positional accuracy. DSM quality degrades exponentially with decreasing CA below 10° [17]. Following this analysis, we initially remove stereo pairs with CA less than 10°, decreasing this threshold iteratively by 1° until an absolute,

stereo-photogrammetric minimum value (CA_{min}) of 3°, below which no useful information is obtainable. Partially and sparsely cloudy images provide more visible surface textures between corresponding features than densely clouded images with abundant successful matches and, as a result, accurate heights over the entire target area. Consequently, selecting less cloudy images can increase the matching success ratio with a reduction in possible blunders and outliers, and decrease computational loads by reducing the number of selected stereo pairs. Since stereo pairs with optimal convergence angles are useless if the images are obscured by clouds, cloud coverage is the primary condition in the stereo pair selection step and is increased iteratively starting from 0% to CL_{max} at increments of 5%. Stereo pairs having temporal baselines of more than 3 h are removed due to the difference in sun elevation angle and shadowing. The mapping condition of tile overlap (Cov) is applied to reduce data voids and to maintain consistent DSM quality by including the minimum number of stereo pairs, nSP_{min}, at each MP. A minimum tile overlap (Cov_{min}) of 30% is needed for inter-plane vertical coregistration to minimize vertical biases through comparison of extracted optimal heights between stereo pairs. The difference in azimuth angles between stereo pairs provides an additional geometric selection criterion. With narrow convergence angles, differences of ~10° or more in azimuth angle significantly degrade DSM quality due to discrepancies between corresponding feature orientations [17]. Due to the configuration of PlanetScope PS2 satellite trajectories, all stereo pairs have azimuth angle differences of 0° or 21°. In multiple stereo pair matching, various viewing geometries may increase DSM quality and minimize height uncertainty. Practically, the removal of stereo pairs composing high azimuth angle differences may lead to data voids and prevent inter-plane vertical coregistration between stereo pairs. In addition, the quality degradation of single-pair DSMs can be minimized by applying the 3D KWEH algorithm utilizing multiple heights. Therefore, the proposed methodology does not utilize differences in azimuth angle for stereo pair selection.

Initial stereo pairs (SP_{init}) are selected based on CA_{min} and the difference in image acquisition times (Td). A map of repeat stereo pair coverage, SP_{map}, is generated from a list of SP_{init} for counting the number of selected stereo pairs at each MP, nSP_{MP}. SP_{map} shares the same array structure as MPs at the pyramid level. If the number of SP_{init} does not exceed two times the value of nSP_{max}, which is the maximum number of stereo pairs at the coarsest pyramid level, the list of SP_{init} is confirmed to execute the SETSM MMP at the coarsest pyramid level. Otherwise, the number of SP_{init} is sequentially reduced, using the filtering and adding processes described below, until all nSP_{MP} exceed the condition $f_s \cdot nSP_{min}$. The filtering step primarily aims to fill the DSM grids by selecting stereo pairs starting from a stereo pair involving the largest tile overlap, regardless of the nSP_{MP}. Based, in order, on the conditional parameters of cloud (CL_{th}), convergence angle (CA_{th}), and tile coverage (Cov_{th}), the filtering step selects half of nSP_{max} in the list of SP_{init}. With starting conditions of the smallest cloud coverage of 0%, the largest CA, and tile coverage of 10° and 100%, stereo pairs are selected through a sequential filtering process which gradually increases cloud coverage at 5% increments and reduces CA and tile coverage by 1° and 5% increments until CL_{th}, CA_{th}, and Cov_{th} reach CL_{max}, CA_{min}, and Cov_{min} of 40%, respectively. Filtered stereo pairs, $SP_{filtered}$, are selected if the conditions are satisfied. The first two conditions of CL_{th} and CA_{th} are fixed when gradually changing Cov_{th}. After Cov_{th} reaches 40%, CA_{th} is reduced by an interval of 1°, and Cov_{th} restarts from its starting value of 90%. When CA_{th} reaches CA_{min}, CL_{th} is increased by an interval of 5%. Then, CA_{th} and Cov_{th} restart from their initial values. If the number of $SP_{filtered}$ exceeds half the value of nSP_{max} during the sequential filtering process, the filtering process is terminated, and a list of $SP_{filtered}$ is confirmed (nSP_{filter} becomes 25% of nSP_{init}). The adding process is performed to satisfy the condition of nSP_{min} for all MPs, assuring consistent DSM quality, which depends on the number

of optimal heights at each MP. Additional stereo pairs, SP_{added}, among the $SP_{initial}$ are selected to satisfy the condition of nSP_{min} at all MPs through a sequential adding process with conditional orders similar to those of the sequential filtering process. In the adding process, the tile coverage threshold for the starting condition is applied as the maximum value between the minimum tile coverage value among the filtered stereo pairs and Cov_{min}, while the ending condition is set to 5%. This strategy seeks to find more available stereo pairs than the filtering process. The other two conditions of cloud coverage and CA are the same as in the filtering process. At each conditional query, the gridded nSP_{MP} values are counted from the tile-coverage map, SP_{map}. When nSP_{MP} exceeds $f_s \cdot nSP_{min}$ and stereo pairs at the MP, SP_{MP}, are not listed in $SP_{filtered}$, SP_{MP} are selected as SP_{added}, where f_s is the safety factor to compensate for uncertainties in the image quality of stereo pairs, as their quality is assessed only after the matching process is complete. Based on testing, a f_s value of 5 ensures the inclusion of potentially good-quality stereo pairs. The final selected stereo pairs, SP_{final}, which include both $SP_{filtered}$ and SP_{added}, are utilized in SETSM MMP to process the coarsest pyramid level. Since both $SP_{filtered}$ and SP_{added} are selected among the list of SP_{init}, the total number of selected pairs does not exceed the number of SP_{init}.

3.1.2. Optimized Stereo Pair Selection with WSPI

After completing the SETSM single stereo-matching procedure at the coarsest pyramid level with all the SP_{final}, stereo pairs with a matching success ratio, MR, of less than 1% are removed from the list, $SP_{final,}$ to filter out low-quality stereo pairs before starting processing of the next pyramid level. The filtered list of stereo pairs is then used as the quality-checked stereo pairs, SP_{check}, to execute the next step in the optimized stereo pair selection. If the number of SP_{check}, nSP_{check}, is less than nSP_{max}, no further steps are required to reduce stereo pairs, and SP_{check} is used to generate the DSM. Otherwise, SP_{map} is updated from the list of SP_{check} and the developed Weighted Stereo Pair Index (WSPI) of each SP_{check} is calculated to prioritize the ranking of stereo pairs by incorporating three geometric and one mapping condition (matching success ratio) of the stereo pairs of the previous level's matching result, as Equation (1).

$$\begin{gathered} WSPI = (0.4 \cdot W_{AA} + 0.4 \cdot W_{CA} + 0.2 \cdot W_{BEA}) \times MR \\ W_{AA} = \left(\frac{AA}{5.0}\right)^{-1.2},\ W_{CA} = \frac{CA^{2.0}}{100},\ W_{BEA} = \frac{1}{|900 - 10 \cdot BEA|^{1.5}} \end{gathered} \tag{1}$$

where W stands for weight. MR is the matching success ratio. The subscripts AA and BEA are the asymmetry angle and the bisector elevation angle of the stereo pair, respectively. If AA is less than 5, AA is set to 5 for W_{AA}. Weights and functions for the three geometric conditions are determined based on the experiments in Section 4.1.2, representing the approximate relationships between DSM accuracy and each geometric condition. The exponent values in the functions are defined through manual evaluation of the quality of single stereo pair DSMs.

The list of SP_{check} is classified into under-counted SP, SP_{under}, and over-counted SP, SP_{over}, by checking nSP_{MP} from SP_{map}. If all nSP_{MP} are less than $3 \cdot nSP_{min}$, all SP_{check} are used to generate the DSM. Otherwise, the stereo pairs in SP_{check} are classified as SP_{under} when the stereo pairs cover any MP where nSP_{MP} is less than $3 \cdot nSP_{min}$. The rest of SP_{check} is classified as SP_{over}, which includes removable stereo pairs based on WSPI to reduce computational loads. Stereo pairs in SP_{over} ranked below the nSP_{max} position in the list of SP_{over}, sorted by WSPI in descending order, are removed from the list of SP_{check} to keep only geometrically well-defined stereo pairs and improve DSM quality. If nSP_{check} surpasses nSP_{max}, a final filtering process is iteratively applied to include wider CA stereo pairs in the DSM processing. This filtering is performed based on only

the CA condition of starting from 10° to 3° at 1° intervals, as explained in Figure 3. In the components of WSPI, the three geometric stereo pair conditions provide global information about the accuracy of stereo pairs and are fixed for all processing pyramid levels. The MR mapping condition provides local information about tile coverage and matching quality and is updated as the SETSM stereo matching process is executed. SETSM iteratively finds optimal heights at increments along the VLL, with increment spacing determining accuracy. This spacing decreases at finer pyramid levels, which improves matching accuracy and minimizes the TIN-constrained search space. Therefore, the matching success ratio of each stereo pair is updated at each pyramid level, providing detailed stereo pair matching quality and tile coverage metrics within the optimized stereo pair selection step.

We demonstrate the stereo pair selection procedure in a cloudy region: the Pantasma crater in northern Nicaragua. We utilize 59 Planet PS2 images with a temporal baseline of 30 days in April 2020, covering a 10 km by 10 km target DSM area (i.e., tile) centered on the crater. Maps of repeat coverage (SP_{Map}) for this target area are shown in Figure 4 for each pyramid level. The initial stereo pair selection, $nSP_{init,}$ of 334 pairs at the coarsest pyramid level, 3, is reduced to a final count, nSP_{final}, of 230 pairs, or close to two times the value of nSP_{max}. Additionally, the minimum and maximum nSP_{MP} for SP_{final} decrease from 55 and 157 for SP_{init} to 48 and 123 pairs, respectively, by retaining a minimum nSP_{MP} close to the limiting value $f_s \cdot nSP_{min}$. The nSP_{final} reaches 100 pairs, with a minimum nSP_{Mp} of 30 pairs at the pyramid levels of 1 and 0. This selection method prioritizes stereo pairs with wider CAs, as shown in Figure 5. Most stereo pairs with a CA of less than 4° are automatically removed from SP_{MP} because they satisfy the geometric, texture, and mapping conditions in these pyramid levels' procedures and WSPI.

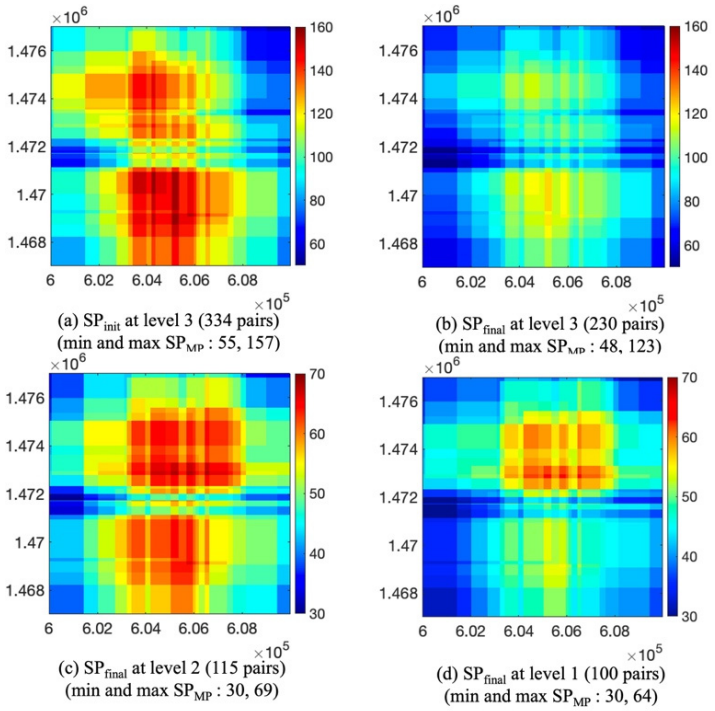


Figure 4. Maps of the number of instances of selected repeat stereo image coverage (SP_{map}) over the Pantasma crater, Nicaragua, area of interest for (**a**) the initial list of stereo pairs (SP_{init}) at the coarsest pyramid level, 3, and (**b**–**d**) the final list of stereo pairs (SP_{final}) for pyramid levels 3, 2 and 1, respectively. SP_{map} at pyramid level 0 is identical to pyramid level 1. Note the change in value range between maps. DSM and its hillshade images are in Figure 6.

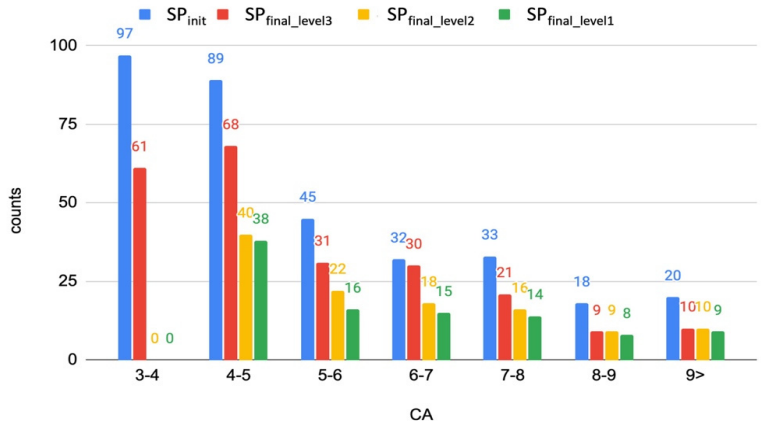


Figure 5. Histogram of selected stereo pair counts according to convergence angle for each pyramid level for the Pantasma crater, Nicaragua, area of interest.

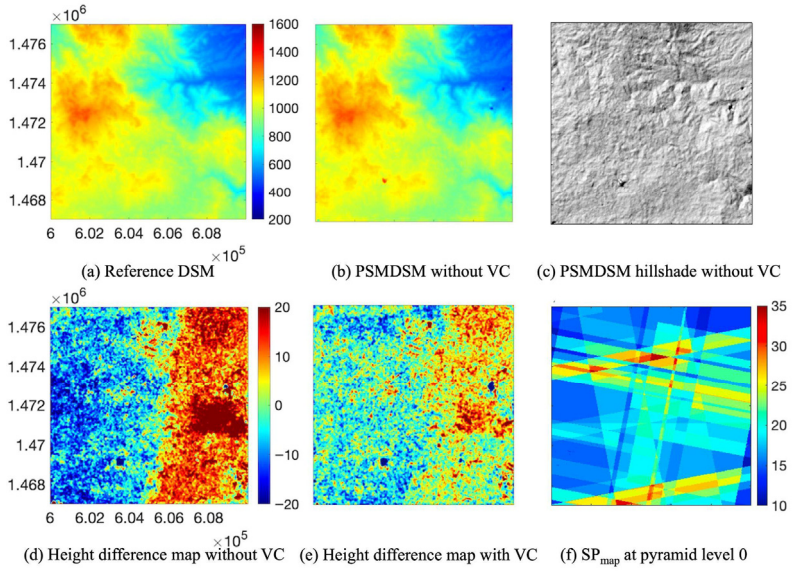


Figure 6. Example of improvement in merged DSM quality through vertical coregistration (VC) for the Pantasma crater area of interest. (**a**) Reference DSM from SRTM. (**b**) DSM created from PlanetScope imagery without VC applied and (**c**) its hillshade rendering. Height differences between the PlanetScope DSM and reference DSM (**d**) without and (**e**) with the VC procedure applied. (**f**) Final map of number of repeat stereo pairs used for DSM construction.

3.2. Inter-Plane Vertical Coregistration

The RPCs in the imagery metadata have biases that result in positional biases between DSMs and offsets in the resulting merged DSM, as shown in Figure 6d. While these vertical offsets can exceed 20 m, they are not detectable in the hillshade image of the resulting merged DSM due to smoothing in the merging process, as shown in Figure 6c. Since, in most cases, stereo pairs are included that partially cover the tile area, reference surfaces entirely covering the tile area must be constructed from these partially covered stereo pairs to remove vertical offsets when GCPs or existing reference DSMs are unavailable. Vertical coregistration (VC) to this constructed reference surface is performed to reduce the vertical biases between stereo pair DSMs before generating the merged DSMs. This step improves consistency in DSM quality (Figure 6e) and enables a robust, fully automated, high-quality DSM processing workflow. We develop a novel inter-plane vertical coregistration to seamlessly and consistently merge PlanetScope PS2 DSMs without GCPs. This is especially important for PS2 DSMs due to large relative height uncertainties resulting from narrow convergence angles compared with the conventional satellite stereo-mode

pairs, as presented in Figure 7. This process consists of two main steps: (1) reference surface construction (DSM_{ref}) and (2) inter-plane VC based on the DSM_{ref}.

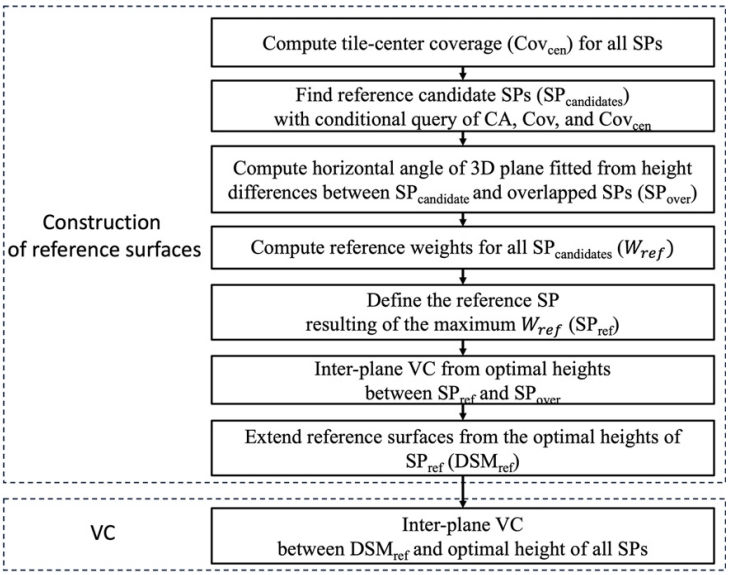


Figure 7. Workflow diagram of the inter-plane vertical coregistration (VC) between surface heights estimated from multiple PlanetScope PS2 stereo pairs.

To estimate the vertical biases between two stereo pairs, overlapped areas are required to provide observations of height differences. In general, partially covered stereo pairs compose various overlapped coverage and topology between stereo pairs as illustrated in Figure 8a. Since not every stereo pair may overlap with each other, sets of contiguously overlapping stereo pairs are grouped, with those groups that overlap the reference stereo pair, SP_{ref}, designated as SP_{over}, and those groups that do not overlap the reference designated as $SP_{no\text{-}over}$. The purpose of the DSM_{ref} construction is to minimize the number of $SP_{no\text{-}over}$ by merging the SP_{over} into the SP_{ref}, so that the entire tile area is fully filled with heights by minimizing the vertical biases. The DSM_{ref} construction step is composed of (1) calculation of tile-center coverage, Cov_{cen}, to select SP_{ref}, which mostly covers the tile center position, (2) selection of reference candidate SPs, $SP_{candidates}$, with conditional query based on CA, Cov, and Cov_{cen}, (3) computation of surface stability of $SP_{candidate}$, that is affected by stereo model scale and defined by the horizontal angle of a 3D plane fitted from height differences between $SP_{candidate}$ and SP_{over}, (4) selection of SP_{ref} as initial DSM_{ref} based on weights representing geometric stability of $SP_{candidates}$, W_{ref}, and (5) expansion of DSM_{ref} by iteratively merging vertical bias-free SP_{over} into SP_{ref}.

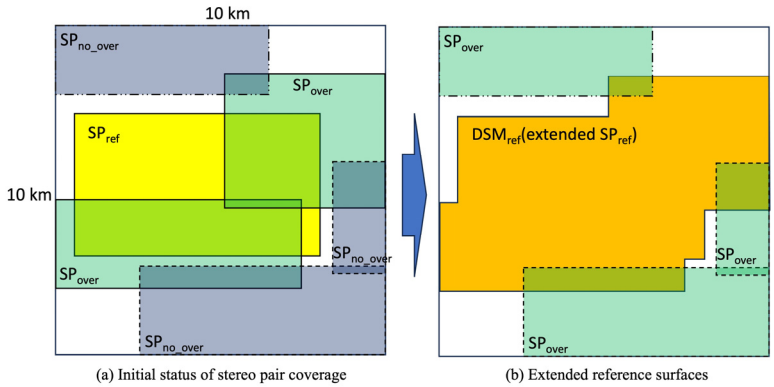


Figure 8. Illustration of tile coverage and topology of stereo pairs. Soild and dashed boxes represent overlapped and not overlapped stereo pairs with the reference stereo pair (SP_{ref}), respectively.

3.2.1. Pairwise Vertical Differences Between SETSM Optimal Heights of Stereo Pairs

SETSM generates each DSM from each stereo pair using both matched (optimal) and unmatched (interpolated) heights at MPs within a TIN structure. For vertical coregistration, pairwise vertical differences are only calculated at the locations of matched optimal heights in both stereo pairs to retain matching accuracy. The distribution of pairwise vertical differences is affected by matching success, determined by image geometry, quality and cloud coverage. As explained in [17] and mentioned above, the height uncertainties resulting from stereo pairs with narrow CA, as typical for PlanetScope PS2 imagery, are more variable than those obtained from conventional satellite images in stereo mode (>30° CA). This large height variation causes fluctuations in the pairwise vertical differences and prevents correct estimation of vertical biases. The degree of fluctuation in vertical differences depends on the pyramid level, which determines image GSDs and height increments in the SETSM algorithm, as well as the viewing geometry that directly affects height uncertainty. In addition, the pairwise vertical bias may not equal the vertical bias calculated from other overlapping DSMs. For example, consider three partially overlapping DSMs labeled A, B and C. The median height difference between A and C will not necessarily equal the sum of differences between A and B and B and C due to spatial variability in height differences and the discrepancy of locations of matched optimal heights. To minimize the vertical bias discrepancy and reduce the effect of clouds or other artifacts, the locations for calculating vertical differences are selected by their histogram with bin edges determined by the average height uncertainty, σ_{az}, of the stereo pairs, as given by

$$\sigma_{az} = \left(\sum_1^{nSP} \sigma_z\right)/nSP = \left(\sum_1^{nSP} \frac{\sqrt{2}\sigma_I}{(B/H)}\right)/nSP = \left(\sum_1^{nSP} \frac{\sqrt{2}\cdot GSD}{2\cdot tan(CA/2)}\right)/nSP \quad (2)$$

where σ_Z is the height uncertainty of the stereo pair, σ_I is the standard error, equivalent to one pixel width, due to the uncertainty in GSD, and B and H are the baselines between the projection centers and flying altitude, respectively.

The value for σ_{az} varies based on the GSD of each pyramid-level image. Therefore, a center histogram bin is defined that ranges from $-\sigma_{az}/2$ to $\sigma_{az}/2$, with the locations of the adjacent left and right bins determined by subtracting or adding σ_{az} from the left and right of the center bin. Optimal height differences are then selected as those contained within a bin with over 30% of its values being the vertical difference values. If no bin's contents contain greater than 30% of these values, the vertical bias adjustment is not applied. By utilizing typically distinct peaks in the height difference distribution, this histogram approach mitigates the influence of noise on vertical coregistration.

3.2.2. Definition of the Reference Stereo Pair

The reference SP, SP_{ref}, should meet two key requirements: sufficient tile coverage to prevent voids in coverage and geometric stability to improve the quality and accuracy in the final PSMDSM. To minimize SP_{no_cover}, we experimentally determined that the reference SP must completely cover a square polygon covering at least ¼ of the tile area and centered on the tile center. The Cov_{cen} is then calculated from the number of optimal heights within this boundary. $SP_{candidates}$ are selected based on conditions of CA, Cov, and Cov_{cen} as described in the sequential filtering process in Section 3.1. In addition to these conditions, the number of SP_{over} with the queried SP is counted to ensure sufficient height difference observations and to expand the SP_{ref} region for generating the DSM_{ref}. A minimum SP_{over} of 3 and fractional overlap for optimal heights between the queried SP and each SP_{over} of 10% are required to derive sufficient observations to accurately estimate vertical biases. SPs satisfying the conditions are selected as $SP_{candidate}$, and this selection procedure is iteratively continued until the number of $SP_{candidates}$ is more than 3.

Single stereo pair DSMs generated from stereo pairs with a CA of less than 10° suffer not only from severe surface noise due to large height uncertainties [17] but also from a scaling issue that results in distortion of horizontal coordinates. Figure 9 shows the height differences between the reference DSM (SRTM) and each single stereo pair SETSM DSM, illustrating the sensitivity of coordinate scaling to view geometry as described by the parameters CA and AA and the BEA. A large AA, primarily caused by the difference in flying altitude or image scale between two images, leads to differences in scaling between the left and right sides of a DSM. This results in increasingly distorted horizontal coordinates with a narrow CA and small BEA. Additionally, this scaling issue becomes more pronounced on steep terrain slopes, as shown in Figure 10, due to differences in distance between surface heights and projection centers at the same ground location. By including only those stereo pairs with wide CAs, small AAs, and large BEAs, as shown in Figure 11, during the $SP_{candidate}$ selection step, the quality and accuracy of PSMDSM can be improved by minimizing the scaling discrepancy, A_{ph}, and surface noise. A_{ph} is a horizontal angle of a plane fitted to the height differences between two DSMs.

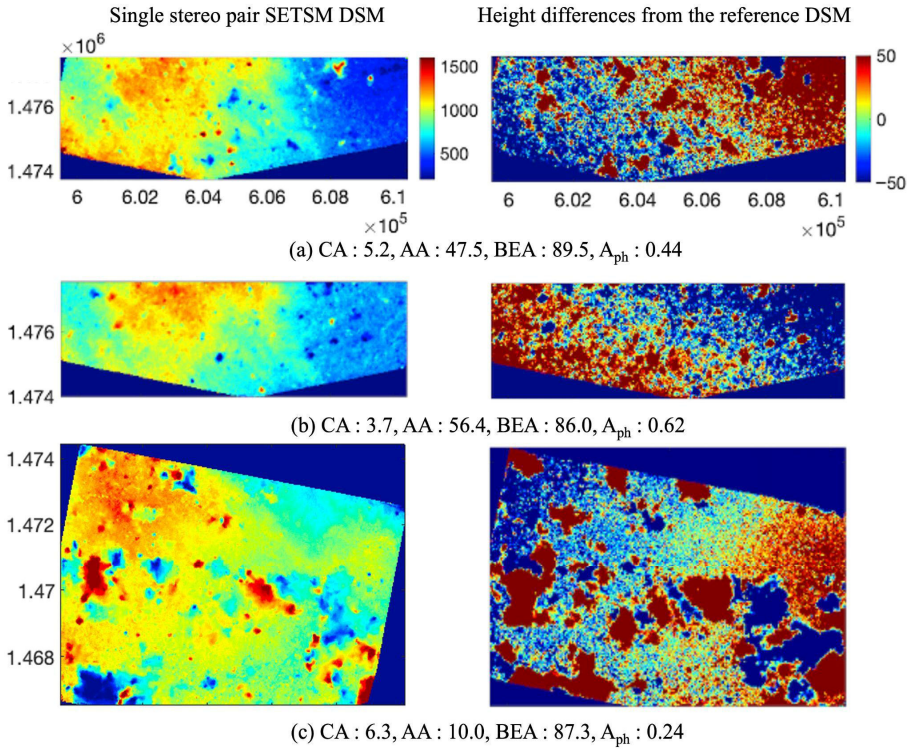


Figure 9. Three examples (**a**–**c**) of (**left**) PS2 DSMs and (**right**) differences in height from the SRTM reference surface for single stereo pairs with large A_{ph}. The distinct DSM blunders are caused by clouds.

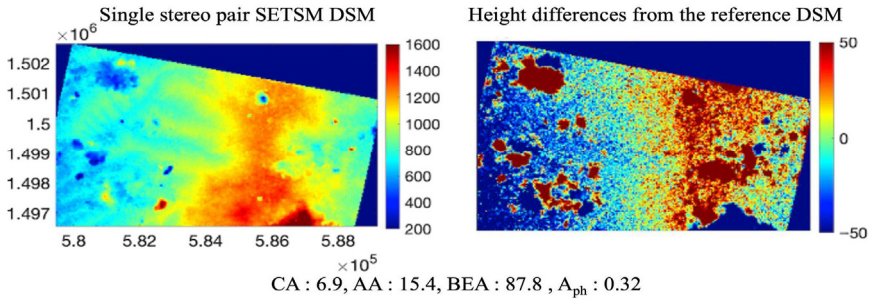


Figure 10. Example of (**left**) PS2 DSM and (**right**) height difference from the SRTM reference surface for a single stereo pair with steep terrain slope, illustrating the increase in difference with surface slope.

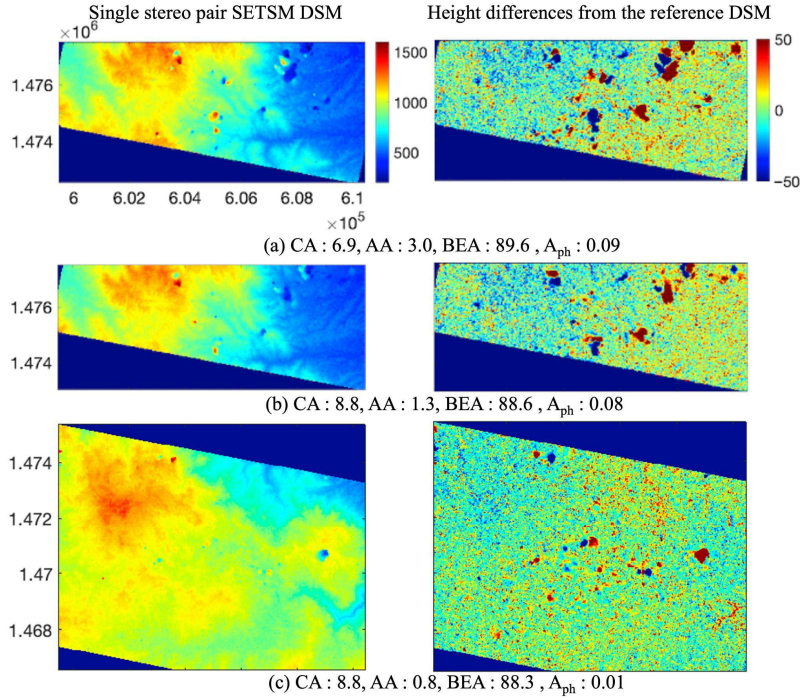


Figure 11. Three examples (**a**–**c**) of (**left**) PS2 DSMs and (**right**) differences in height from the SRTM reference surface for single stereo pairs with a relatively small A_{ph}. The distinct DSM blunders are caused by clouds.

To evaluate the scaling discrepancy for inter-pairs, $IP_{cand\_over,}$ formed between $SP_{candidate}$ and the corresponding SP_{over}, we first obtain the horizontal angle (°), A_{ph}, of a plane fitted to the height differences in IP_{cand_over}. As shown in Figures 9–11, A_{ph} ranges from 0 to several degrees, depending on geometric conditions as well as terrain slope and elevation. Then, a reference weight, W_{ref}, for $SP_{candidate}$ is computed by incorporating its Weighted Stereo Pair Index (WSPI), matching the quality of NCCs and the average pairwise scaling discrepancy, A_{ph}:

$$\begin{aligned} W_{ref} = & \left(0.4 \cdot \frac{WSPI}{MR} + 0.2 \cdot avg_{\rho} + 0.4 \cdot \frac{\sum W_{pha}}{nSP_{over}}\right) S_f \\ & W_{pha} = 1 - \left(200 \cdot A_{ph}^2\right) \end{aligned} \quad (3)$$

where nSP_{over} is the number of SP_{over} corresponding to $SP_{candidate}$, and avg_{ρ} is the average value of SETSM Normalized Cross-Correlation (NCC) of all matched features in a stereo pair. S_f is the scaling factor used to normalize the optimal height weights in the 3D KWHE algorithm to a maximum value of 100, as described in Section 3.4.

The value of W_{ph} is set to 0 when W_{ph} is less than 0 and avg_{ρ} is applied as the uncorrected NCC (UNCC) if UNCC is greater than the value of the geometrically corrected NCC (GNCC) in SETSM. SP_{ref} is then selected when its W_{ref} is the maximum value among all $SP_{candidate}$. To improve the accuracy of W_{ref}, IP_{cand_over} whose A_{ph} values rank within the lowest five among the list of IP_{cand_over} are only applied in the calculation of W_{ref}, when the number of IP_{cand_over} exceeds five. As a result, the five corresponding SP_{over} and the determined SP_{ref} are utilized to generate DSM_{ref}. The remaining SP_{over} are classified as SP_{overR} and are used in the next step of VC.

3.2.3. Construction of Reference Surfaces, DSM_{ref}

Based on SP_{ref} and its corresponding SP_{over}, DSM_{ref} is iteratively updated and expanded starting from SP_{ref} through VC, as shown in Figure 12. To remove vertical biases

of SP_{over} relative to SP_{ref} and remove possible poor stereo pairs in the list of SP_{over}, VC is performed by Weighted Least Squares Adjustment (WLSA). The height differences for IP_{ref_over}, dH1; IP_{ref_overR} between SP_{ref} and SP_{overR}, dH2; and IP_{over_over} between SP_{over} and SP_{over}, dH3, are calculated based on the maximum histogram bin, as described in Section 3.2.1. Vertical bias observations, dH_{avg}, are calculated by averaging the height differences, and standard deviations of dHs, dH_{σ}, are used to weight these observations. A plane is fitted to each IP height difference to estimate an A_{ph}. This value is compared against the overall distribution of A_{ph} to remove stereo pairs that perform poorly relative to SP_{ref}. During the iterative SETSM procedure at each pyramid level, the mean and standard deviation of A_{ph} are updated, and stereo pairs falling outside the 99% confidence interval of A_{ph} are classified as outliers and excluded from VC processing. The large height uncertainty of the single stereo pair PlanetScope DSM leads to height fluctuations of several tens of meters at the same locations across different SPs. This uncertainty can introduce inconsistent vertical biases for a single SP_{over} when the locations used for height differencing in dH1 and dH2 are not identical. To mitigate potential divergences or failures in vertical bias adjustment caused by this uncertainty, a weighted adjustment is applied, considering both the residuals of observations and the variations in height differences. To enforce the condition of the set of observations dH1 to be a reference, their weight is set to a relatively large value (W_{max}; 10,000) because SP_{over} satisfies the conditions of W_{ref}. The weights of dH2 and dH3 are calculated as

$$\begin{aligned} W_{dH2} &= 1 + (1/\sigma_{res\_overR} + 1/\sigma_{dH2})/2 \\ W_{dH3} &= (1/\sigma_{res\_overF} + 1/\sigma_{dH3\_F})/2 + (1/\sigma_{res\_overS} + 1/\sigma_{dH3\_S})/2 \end{aligned} \quad (4)$$

where σ_{res_overR}, σ_{res_overF} and σ_{res_overS} are the standard deviations of adjusted residuals for the stereo pairs corresponding to SP_{overR} for dH2 and the first and second stereo pairs in IP_{over_over} for dH3, respectively, and initialized as 1.0 before weighted adjustment is performed. F and S stand for the first and second stereo pair, respectively. σ_{res} is calculated by collecting all adjusted residuals corresponding to the stereo pair in observations. σ_{dH} is the standard deviation of dHs. Values of σ greater than 1 m are set to 1 m.

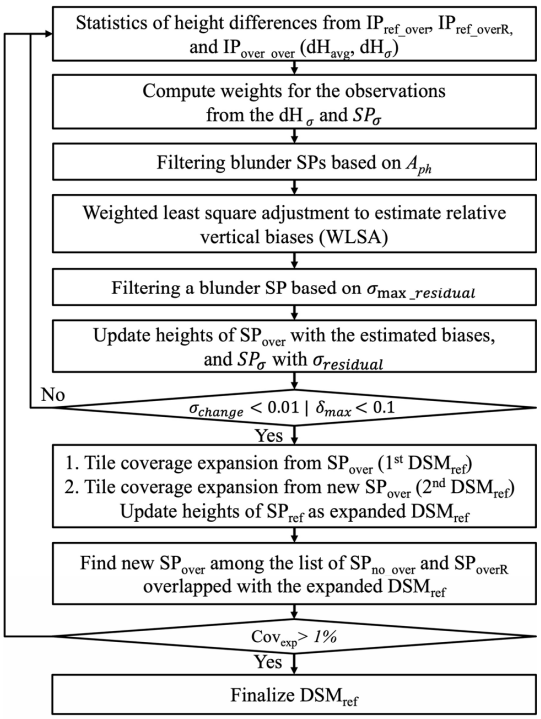


Figure 12. Workflow for generating the DSM_{ref}.

With the measured vertical biases of $dH1_{avg}$, $dH2_{avg}$, and $dH3_{avg}$, the unknown vertical biases for SP_{over} and SP_{overR}, and the weights for the dH2 and dH3 observations, WLSA is executed as

$$X = \left(A^T W A\right)^{-1} A L$$

$$X_{(5+p)\times 1} = \begin{bmatrix} dH_{O1} \\ dH_{R2} \\ dH_{O2} \\ dH_{R2} \\ \vdots \\ dH_{O5} \\ dH_{R5} \\ \vdots \\ dH_{Rp} \end{bmatrix}, \; A_{q\times(5+p)} = \begin{bmatrix} -1 & 0 & 0 & 0 & 0 & 0 & 0 & 0 & 0 \\ 0 & -1 & 0 & 0 & 0 & 0 & 0 & 0 & 0 \\ 1 & 0 & 0 & -1 & 0 & 0 & 0 & 0 & 0 \\ 0 & 0 & -1 & 0 & 0 & 0 & 0 & 0 & 0 \\ 0 & 0 & 0 & -1 & 0 & 0 & 0 & 0 & 0 \\ 0 & 0 & 1 & 0 & 0 & -1 & 0 & 0 & 0 \\ & & & & \vdots & & & & \end{bmatrix} \tag{5}$$

$$W_{q\times q} = \begin{bmatrix} W_{\max} & 0 & 0 & 0 & 0 & 0 \\ 0 & W_{dH2\_R1} & 0 & 0 & 0 & 0 \\ 0 & 0 & W_{dH3\_O1O2} & 0 & 0 & 0 \\ 0 & 0 & 0 & W_{\max} & 0 & 0 \\ 0 & 0 & 0 & 0 & W_{dH2\_R2} & 0 \\ 0 & 0 & 0 & 0 & 0 & W_{dH3\_O2O3} \\ 0 & 0 & 0 & 0 & 0 & \ddots \end{bmatrix}_{q\times q}, \; L_{q\times 1} = \begin{bmatrix} dH1_{avg\_O1} \\ dH2_{avg\_R1} \\ dH3_{avg\_O1O2} \\ dH1_{avg\_O2} \\ dH2_{avg\_R2} \\ dH3_{avg\_O2O3} \\ \vdots \end{bmatrix}_{q\times 1}$$

where X, W, A, and L denote the unknown parameter, weight, coefficient, and observation matrices, respectively. p and q represent the number of SP_{overR} and observations corresponding to $dH1_{avg}$, $dH2_{avg}$, and $dH3_{avg}$, respectively. The number of observations is determined by the number of SP_{over}, SP_{overR} and $dH3_{avg}$ associated with IP_{over_over}. The number of unknowns is defined as the sum of the number of selected SP_{over} (up to a maximum of five) and SP_{overR}. Subscripts O and R indicate the indices of SP_{over} and SP_{overR} respectively. W is the weight calculated from Equation (4) according to SP indices.

Residuals are calculated from the adjusted vertical biases and are grouped according to the list of unknowns. The grouped residuals for the unknowns are utilized to calculate the standard deviations of σ_{res}s for the unknown of the stereo pair. An outlier SP relative to SP_{ref} is sequentially selected among the list of SPs when the resulting σ_{res} is outside of the 90% confidence interval of the WLSA calculated by multiplying the σ_0 of WLSA by 1.65. Then, the SP with the maximum σ_{res} is removed for the next iteration. After adjusting the relative vertical biases of SP_{over} and SP_{overR}, the height differences are recalculated from the updated heights of SP_{over} and SP_{overR} for the next adjustment. The WLSA is terminated when the change ratio of the σ_0 of WLSA between each iteration, σ_{change}, is less than 0.01 or the maximum adjusted amount for the unknown, δ_{max}, is less than 0.1 m. If the terminating conditions are not satisfied and the number of iterations reaches the maximum number, which applies to prevent a divergence-induced infinite loop, the SP_{ref} is replaced with the next $SP_{candidate}$ corresponding to the next-highest W_{ref} position. The bias-free heights of the retained SP_{over} are then utilized to expand the coverage of SP_{ref}, filling voids in the tile and constructing the initial version of the DSM_{ref}. The lists of SP_{over} and SP_{overR}, $SP_{updated}$, are updated by selecting stereo pairs that overlap with the 1st DSM_{ref}. $SP_{updated}$ is then added into the WLSA procedure to minimize vertical biases relative to the DSM_{ref} and to eliminate potential outlier stereo pairs. Subsequently, the next tile coverage expansion procedure to construct the 2nd DSM_{ref} is processed by sequentially attaching $SP_{updated}$ into

the 1st DSM_{ref}. The $SP_{updated}$ with the highest W_{ref} and a tile coverage incremental ratio of more than 1% is selected, and its vertical bias-free heights are integrated into the 1st DSM_{ref} to achieve the purpose of filling the void spaces of the tile and improving DSM_{ref} quality. With the expanded 2nd DSM_{ref}, the observations for WLSA are updated using the new revised $SP_{updated}$. This tile-coverage expansion procedure is iteratively performed until the tile coverage incremental ratio for $SP_{updated}$ is less than 1%. The finalized DSM_{ref} is the reference surface for compensating vertical biases in all SPs over the tile region.

3.2.4. Sequential Vertical Coregistration with the Reference DSM

Based on the generated DSM_{ref} or an existing reference DSM, the inter-plane VC is applied to estimate the vertical biases of the optimal heights of all SPs, and a sequential procedure prevents failure or divergence of the adjustment model due to large height uncertainties. All SPs are evaluated based on the A_{ph} condition to remove poor stereo pairs. Based on the results of the WLSA with SP_{ref} and its corresponding SP_{over} during DSM_{ref} generation, as described in Section 3.2.3, each SP not included in SP_{over} and the overlapping DSM_{ref}, SP_{added}, is added into the adjustment model sequentially in order of descending convergence angles to increase the accuracy of the adjustment model and to select well-defined SPs in PSMDSM generation. Then, all possible height differences between DSM_{ref}, SP_{over}, and SP_{added} are calculated, and corresponding weights are calculated from Equation (4). With the observations of height differences and weights, the WLSA is iteratively performed with the termination conditions provided in Section 3.2.3, and the SP_{added} is removed as an outlier from the vertical coregistration and SETSM MMP if the termination conditions are not satisfied due to a large height uncertainty. When SP_{added} is successfully registered by the WLSA, it is added to the list of SP_{over} and is held constant in subsequent WLSA. The same sequential process is performed by adding another SP in order of descending convergence angle.

3.3. Weighted Optimal Heights with 3D KWHE Algorithm

A 3D kernel-based weighted height estimation (3D KWHE) algorithm is developed to estimate the final optimal heights from the multiple optimal heights of all the pairs at all MPs [16]. This algorithm applies a 3D, adaptable kernel-based height estimation technique to improve the statistical reliability of the final optimal heights. It prioritizes multiple height estimates based on geometric conditions to improve the quality of merged DSM from multiple stereo pair DSMs after removing vertical biases between stereo pair DSMs. 3D KWHE comprises two main procedures, as described in Figure 13. The first procedure involves 1D height-interval processing in the vertical direction to estimate the most reliable optimal height at each MP. The second procedure involves 2D kernel-based processing on the XY horizontal plane for neighborhood-connected height estimation and surface noise reduction through the Local Surface Fitting (LSF) algorithm.

In the 3D KWHE algorithm for PSMDSM generation, the weights of optimal heights, WM_{oh}, are replaced with W_{ref} incorporating the Weighted Stereo Pair Index (WSPI), matching quality of NCCs, and the A_{ph}, as explained in Equation (3). After removing the averaging bias between stereo pair DSMs through the VC step, scaling distortion errors still remain in each DSM. The A_{ph} indicates the magnitude of these scaling distortion errors and is applied to assign weights for heights estimated from individual stereo pair DSMs. Then, the integrated weights for WH_q, $IWHq$, are calculated through a weighted summation of the WM_{oh} and the distance weights, W_{dist}, of the S_{oh}, following a modified formulation from [16] to constrain the value range:

$$IWHq = \sum_{1}^{nSoh} \left(\frac{WM_{Soh} + W_{dist}}{2}\right),\ W_{dist} = \frac{s_f}{(Std_{dist}/HI)^{0.6}} \quad (6)$$

where WM_{Soh} is the reference weight, W_{ref}, for S_{oh}, and W_{dist} is the weight for the Euclidean distance between optimal heights, including S_{oh} and Q_{oh}. Std_{dist} is the standard deviation of the Euclidean distance between the query S_{oh} and the rest of S_{oh} and Q_{oh}. nS_{oh} is the number of S_{oh}.

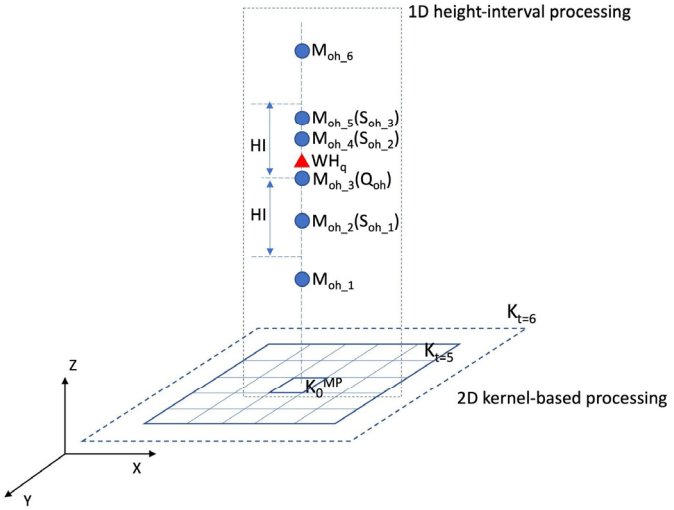


Figure 13. Schematic illustration of the 3D kernel-based weighted height estimation (KWHE) consisting of 1D processing in the vertical direction, z, at each MP, and 2D kernel-based processing on the xy plane. The variable *HI* is the height interval; M_{oh} are the multiple optimal heights; Q_{oh} is the query optimal height for calculating a weighted optimal height, WH_q; S_{oh} are the selected optimal heights within the *HI* for the query optimal height (Q_{oh}). K_t^{MP} defines the 2D kernel with t size centered around a target MP (K_0^{MP}). Adapted from [16].

Based on the integrated weights and weighted optimal heights at each MP, 2D kernel-based processing generates the final weighted optimal heights at each MP, $FWOH_{MP}$, as described in [16]. A merged bias-free DSM generated from $FWOH_{MP}$ is iteratively updated at each pyramid level's procedure, and its quality and accuracy are progressively improved as the pyramid level becomes finer.

3.4. RPC Bias Compensation Based on Bias-Free DSM

A merged, bias-free DSM is utilized as a reference DSM for compensating RPC bias between each stereo pair. Biases in RPCs degrade DSM quality in SETSM due to misalignment of the vertical line locus between two images. The biases in a single stereo pair can be relatively compensated for by iteratively reducing the misalignment between matched features derived from SETSM within the process for each pyramid level, increasing the number of recovered optimal heights and DSM quality [16]. The relative biases of a single stereo pair are individually compensated based on the bias-free DSM heights at each MP, which act as virtual GCPs. The locations of virtual GCPs are projected into image points in both the left and right images of a stereo pair by the provided RPC model. As described in [20], image points on the left image are fixed, and the relative RPC biases of the right image are estimated through spatial cross-correlation. An investigation into the relationship between relative RPC biases and DSM object translations using WorldView stereo imagery found that the vertical translation component, T_z, has a strongly linear relationship with relative RPC biases, while horizontal translations show only small variations (~0.3 m), which were within several pixels of RPC biases [20]. Thus, based on that analysis, relative biases between individual RPC images result mostly in vertical, rather than horizontal, biases between DSMs. Therefore, RPC bias compensation with a bias-free DSM primarily aligns vertical shifts based on the horizontal accuracy of the reference DSM (DSM_{ref}) of the vertical coregistration. The stereo pair bias corrections are applied to the RPC model for the next iteration to remove the coregistration

error between stereo pairs. The remaining horizontal biases in stereo pairs are minimized when determining weighted optimal heights within the 3D KWHE algorithm.

3.5. Tile Mosaic

The DSM tiles are then aligned and merged into a seamless mosaic. First, the tiles are aligned in the horizontal and vertical directions to remove relative offsets. This is done by applying least squares adjustment to the offsets between each tile and the surrounding tiles, as obtained from the overlapping borders (i.e., buffers). The three-dimensional offsets between each neighboring tile are estimated using the approach of [21]. Very large offsets (>50 m) due to noisy surfaces, such as from clouds or water, are ignored when calculating the least squares adjustment. Following the three-dimensional adjustment, linear distance-weighted blending is applied to the overlapping border area to remove any remaining offsets and ensure a seamless merge at the tile borders.

4. Experimental Results

4.1. Pantasma Crater, Nicaragua

Over 10 km in diameter, the Pantasma crater (13°22′N and 85°57′W) is among the major hypervelocity impact structures discovered in the past decade and only the fourth crater of that size to be found in South America [22], and its structure has been investigated to understand its impact origin through quantitative analysis of the Shuttle Radar Topographic Mission (SRTM) 90 m digital elevation model and fieldwork to collect rock and soil samples [23]. In addition, the Pantasma impact crater was the source of the impact glass tektite that was documented 530 km away in Belize [24]. We selected the Pantasma crater as an experimental test region to support geological and topographical research by providing a large-scale PlanetScope PS2 DSM mosaic at higher resolutions than currently available from InSAR sensing in a persistently cloudy region. The target region of 70 km by 60 km (7 by 6 tiles) ranges between 580,000 m and 650,000 m for the X, and 1,447,000 m and 1,507,000 m for the Y, coordinates projected by UTM zone 16N, respectively, as shown in Figure 14.

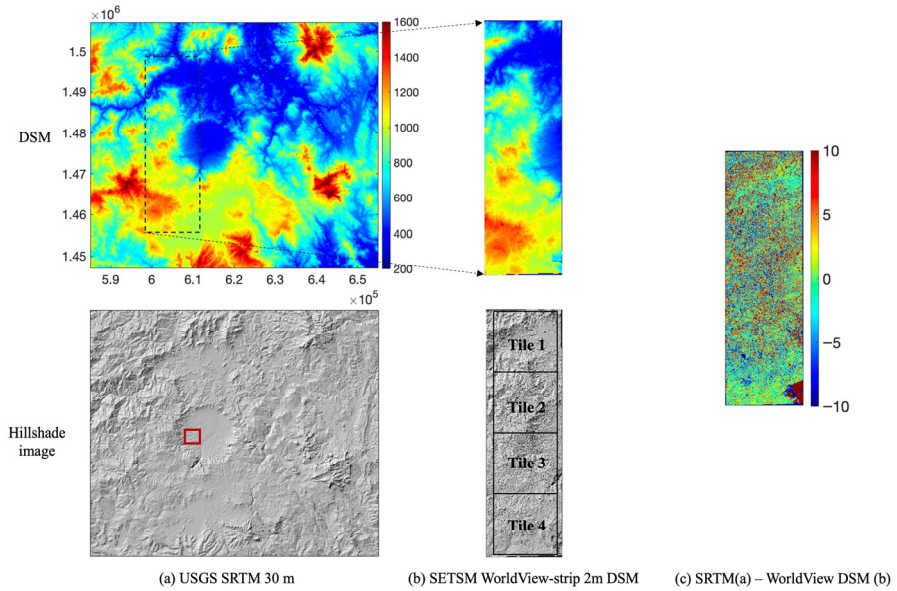


Figure 14. Reference DSM (**top**) colorscale and (**bottom**) hillshade rendering for the Pantasma crater test site: (**a**) USGS SRTM 30 m DSM in 2000, (**b**) SETSM WorldView3 stereo pair 2 m DSM in 2020. (**c**) The height differences between SRTM and WorldView DSM. DSM translations of SETSM DSM are −14.21 m, 21.23 m, −1.52 m. The red box area is selected for a detailed comparison with the hillshade image, as shown in Figure 15.

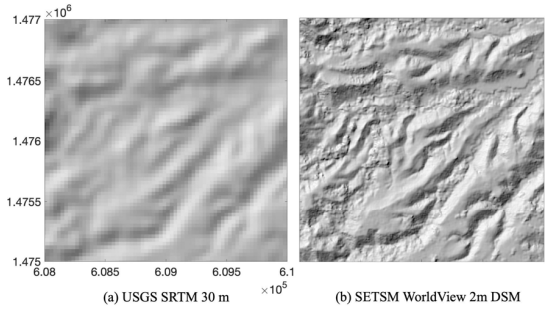


Figure 15. Zoomed-in area in the red rectangle in Figure 14a showing comparison of surface feature resolution between (**a**) SRTM 30 m and (**b**) SETSM 2 m DSM hillshade renderings.

4.1.1. Reference Data and PlanetScope PS2 Images

The USGS Earth Resources Observation and Science (EROS) Center provides 1 arc (~30 m) SRTM digital elevation models covering this area, and two tiles (SRTM1N13W086V3 and SRTM1N13W087V3) are merged to provide the Pantasma carter reference DSM. SRTM data were acquired on 11 February 2000 (USGS EarthExplorer, https://earthexplorer.usgs.gov/, accessed on 26 December 2025) [25]. The SRTM DSM is used as a regional baseline and for absolute vertical alignment. A cloud-free WorldView-3 image stereo pair acquired during a single orbital pass (i.e., in-track stereo mode) on 30 April 2020 is utilized to generate a SETSM 2 m DSM as the primary high-resolution validation benchmark for PlanetScope DSM accuracy. In Figure 14d, the height differences between the SRTM 30 m and SETSM 2 m DSM are calculated after 3D coregistration using the geometric constraints method of [26]. Height differences are caused by differences in resolution, SRTM backscatter and photogrammetric surface heights over vegetation and actual changes in the surface, including seasonal changes in vegetation between February and September, as described in Figure 15. The right bottom outliers in the SETSM 2 m DSM are caused by water surfaces on lake Apanas in Figure 14c.

Using the API, we downloaded a total of 1285 PlanetScope PS2 images over the study area acquired between March and June 2020 and with a cloud cover of less than 50% using the API. Both PlanetScope PS2 single-pair stereo (PSSDSMs) and multi-pair stereo DSMs (PSMDSMs) with 4 m postings were generated for quality analysis and comparison.

4.1.2. Geometric Sensitivity Analysis for Quality of PlanetScope PS2 Single Stereo DSMs

PSSDSMs are generated utilizing the stereo pair SETSM procedure to evaluate DSM quality in relation to the viewing geometry parameters of AA, BEA, and CA, as well as the DSM scaling error represented by A_{ph}, which reflects the stability of the coordinate system in the DSM. A total of 10 tiles, including the 4 tiles overlapping the SETSM WorldView3 reference DSMs, are selected to configure 928 stereo pairs. To maintain spatial consistency in the analysis, we use the 817 PSSDSMs that cover at least 80% of the tile. Figure 16 describes the distribution of RMSE of height differences, $RMSE_{dH}$, between PSSDSMs and the reference DSMs according to AA, BEA, CA, and A_{ph}. In the relationship between $RSME_{dH}$ and AA, as illustrated in Figure 16a, PSSDSM quality is highly sensitive to AA due to its constraint on the maximum achievable accuracy of PSSDSM, as shown by the line B_{AA} in Figure 16a. Accordingly, an AA of approximately 30° can yield PSSDSMs with $RMSE_{dH}$ as low as 15 m. BEA exhibits a weaker, but significant, correlation with $RMSE_{dh}$ compared to AA, with a maximum expected accuracy defined by the line B_{BEA} in Figure 16b. As expected, $RMSE_{dH}$ increases with greater DSM scaling error, quantified by A_{ph}. In Figure 16c, larger A_{ph} values, which result from combinations of large AAs and small BEAs, correlate with a decrease in height accuracy, with the maximum expected accuracy given by the line of B_{Aph}. Figure 16d illustrates the critical role of the CA, which

defines the achievable minimum and maximum bounds of PSSDSM accuracy, with a band width of approximately 15 m of $RMSE_{dH}$ bounded by a lower bound, LB_{CA}, and upper bound, UB_{CA}. In the case of stereo pairs with 8° CA, PSSDSM $RMSE_{dH}$ ranges from 10 to 25 m depending on the specific combinations of AA and BEA. To derive more detailed relationships, an interval-based analysis is performed by grouping the stereo pairs by $RSME_{dH}$ at 3 m intervals. For each group, the mean and standard deviation values of AA, BEA, A_{ph} and CA are calculated and presented in Figure 17. As shown in Figure 17a, $RMSE_{dh}$ exponentially increases with a rising trend in the AA mean. Additionally, large $RMSE_{dh}$ values are associated with high variability in AA, ranging from 1.56 m to 18.67 m. In the case of the BEA, most stereo pairs have BEA values between 86° and 90°, with a mean of 88° and a standard deviation of approximately 1°, as shown in Figure 17b. Compared to the AA mean variance, which ranges from 2.48° to 40.81°, a small decrease in the BEA significantly degrades the quality of PSSDSMs, indicating a high sensitivity of $RMSE_{dh}$ to decreasing BEA. The relationship between the A_{ph} mean and $RMSE_{dH}$ in Figure 17c demonstrates a clear linear correlation with a slope of approximately 0.01° per 1 m increase in the $RMSE_{dh}$. The variance in A_{ph} also increases linearly with $RMSE_{dH}$, reflecting a growing instability of the coordinate system in lower-quality DSMs. Figure 17d explains the inverse relationship between CA mean and PSSDSM quality. The variability in CA is more stable, with standard deviations ranging from 1.14° to 2.73°, compared to AA and A_{ph}.

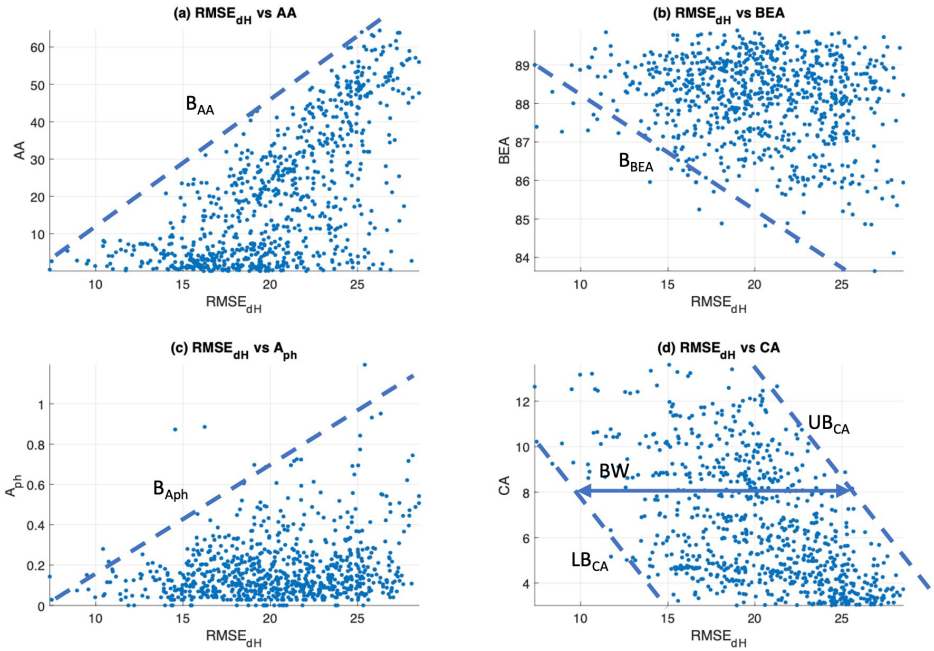


Figure 16. Scatter plots of single stereo pair PS2 DSM root mean squared error in height ($RMSE_{dH}$) and stereo pair geometric parameters (**a**) AA, (**b**) BEA, (**c**) A_{ph} and (**d**) CA. Dashes in (**a**–**c**) are the empirical limit functions B, whereas in (**c**), the dashes denote the ranges LB_{CA} to UBc_A.

To investigate how viewing geometry contributes to distortion in the DSM coordinate system resulting from the scaling problem described in Section 3.2.2, the viewing geometry parameters of AA, BEA, and CA are analyzed in relation to A_{ph}, as shown in Figure 18. Figure 18a–c show the distribution of A_{ph} with respect to each parameter, while Figure 18d–f present the mean and standard deviation values of the parameters within 0.1° intervals of A_{Ph}. As shown in Figure 18a, AA ranging from 0° to 60° are mostly distributed across A_{ph} between 0° and 0.2°, and AA values less than 10° result in A_{ph} values exceeding 0.6°. The mean and standard deviation of AA within each A_{ph} interval remain relatively stable, as presented in Figure 18d. Similarly, Figure 18b indicates that large

BEAs can also lead to increased scaling error, and the corresponding statistics across A_{ph} intervals exhibit a consistent and even distribution, as shown in Figure 18e. Compared to the AA and BEA, the CA demonstrates a strong inverse relationship with A_{ph}, as depicted in Figure 18f, and effectively bounds the upper limit of A_{ph}, represented by the line of B_{Aph2} in Figure 18c. These results suggest that the scaling error of the PSSDSM coordinate system is not driven by a single geometric parameter but rather by the combined effects of the AA, BEA, and CA. In addition, the computation of A_{ph} is significantly influenced by terrain relief, as shown in Figure 10. Based on this analysis, the weight functions of Equations (1) and (3) are empirically derived by integrating A_{ph}, viewing geometric parameters, and image-matching quality.

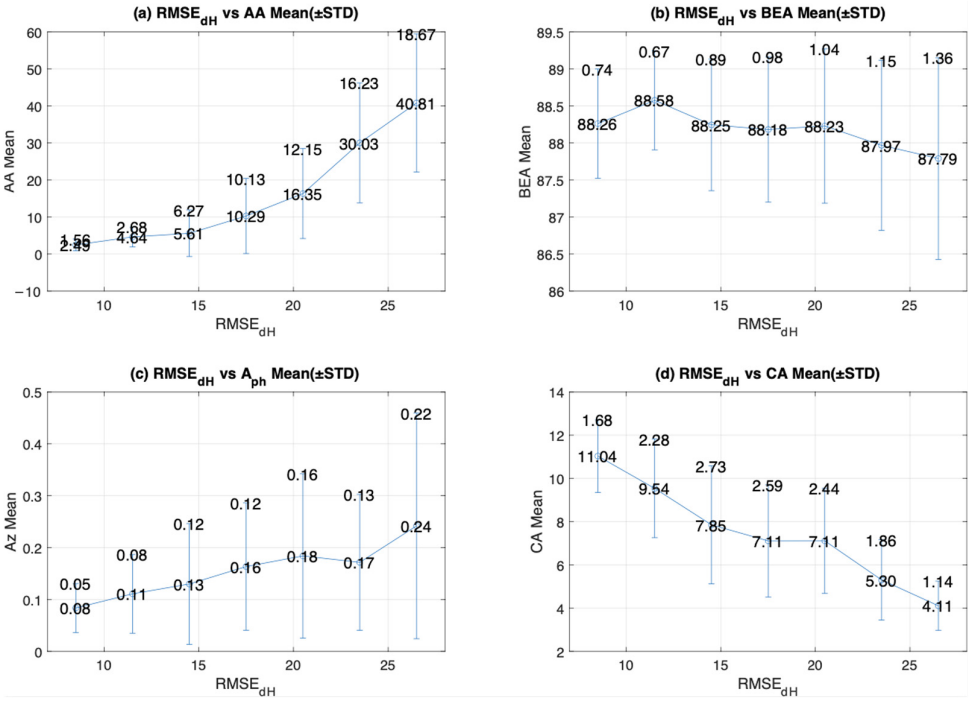


Figure 17. Same as in Figure 16, but with (**a**) AA, (**b**) BEA, (**c**) A_{ph} and (**d**) CA averaged in 3 m bins of $RMSE_{dH}$. Vertical bars are the standard deviations.

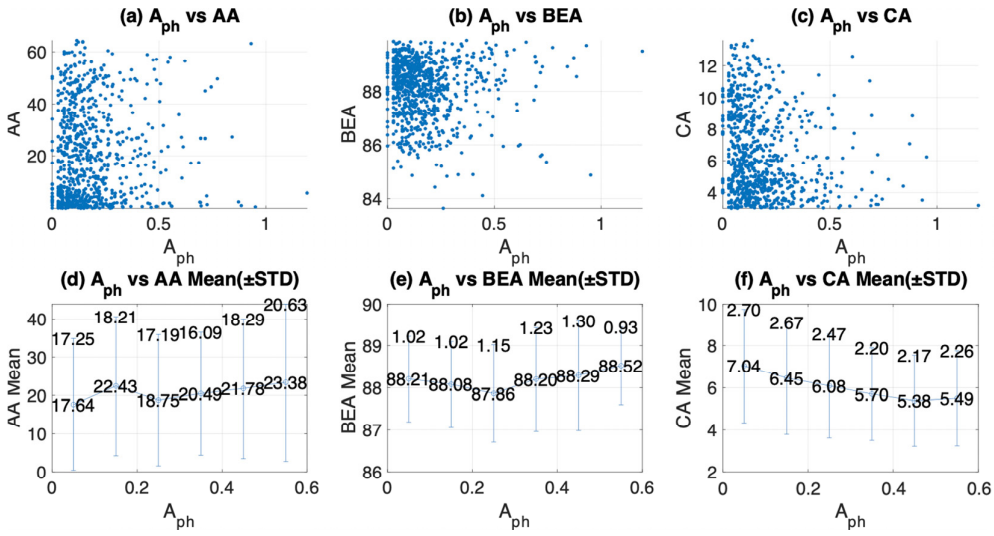


Figure 18. Scatter plots between A_{ph} for single-pair PS2 DSMs geometric parameters (**a**) AA, (**b**) BEA and (**c**) CA. (**d**–**f**) Same data as (**a**–**c**) but averaged within 0.1 increments of A_{ph}. Vertical bars are the standard deviations.

4.1.3. PSMDSM Comparison to WorldView-3 DSM

Here, we compare the PSMDSMs to the overlapping and coincident 2 m resolution DSM created from a stereo pair of submeter-resolution WorldView-3 images described in Section 4.1.1.

Analysis of Stereo Pairs and VC WLSA

As described above, candidate PlanetScope PS2 images overlapping the WorldView3 2 m reference DSM are selected from the Planet API to form stereo pairs with >3° CA, <50% cloud coverage, and >30% overlap and a maximum temporal baseline of 30 days between April 1st and 30th. Since the reference WorldView3 DSM region is 13 km by 43 km, DSMs are generated in four 10 km by 10 km square tiles covering this area, as shown in Figure 14b. Table 1 shows the number of candidate (or initial) and final selected images to generate each PSMDSM tile. Although the candidate images include 10 to 21 images with more than 30% cloud coverage, the proposed, optimized stereo pair selection procedure efficiently removes excessively cloudy images in the matching process, with 80% of selected images having less than 10% cloud coverage. The optimized stereo pair selection automatically prioritizes images with less cloud coverage, while a few images with greater than 30% cloud cover are applied to cover Tiles #2, #3, and #4. In the case of Tile #1, 39 out of 67 images are applied to generate the DSM, all with less than 30% cloud coverage, removing all 10 images with a cloud coverage over 30%.

Table 1. The number of the initial and selected images to generate PSMDSMs with 4 tiles with respect to cloud coverage. 'Initial', 'Final', and 'Applied Ratio' stand for the number of candidate images and final images selected for DSM generation and the ratio of the selected images to the initial images, respectively.

CL	Tile #1			Tile #2			Tile #3			Tile #4		
	Initial	Final	Applied Ratio	Initial	Final	Applied Ratio	Initial	Final	Applied Ratio	Initial	Final	Applied Ratio
0~10	28	24	85.7	29	24	82.8	25	22	88.0	28	24	85.7
10~20	15	10	66.7	13	13	100.0	4	3	75.0	4	1	25.0
20~30	14	5	35.7	14	10	71.4	12	7	58.3	12	7	58.3
30~40	6	0	0.0	7	2	28.6	14	4	28.6	13	4	30.8
40~50	4	0	0.0	5	3	60.0	4	1	25.0	8	2	25.0
Total	67	39		68	52		59	37		65	38	

Table 2 presents the number of SP_{final} at the coarsest and finest pyramid levels, classified by the viewing geometry parameters of the CA, AA, and BEA. The PSMDSMs are iteratively updated starting from pyramid level 3, where the original 4 m resolution images are resampled to 32 m resolution Gaussian pyramid images, down to pyramid level 0 at the full original image resolution. More than 230 nSP_{final} at level 3 are reduced to 100 nSP_{final} at level 0 through the optimized stereo pair selection step. This reduction is achieved by removing all stereo pairs with a CA less than 4°, while retaining most stereo pairs with a CA greater than 8°. Moreover, stereo pairs with an AA greater than 40° and BEA less than 86°, which are conditions that degrade PSSDSM quality, as explained in Section 4.1.2, are automatically and efficiently minimized to ensure high-quality PSMDSMs. About 50% of stereo pairs with a less than 10° AA at level 3 are not included in SP_{final} at level 0 due to their insufficient tile coverage and high cloud coverage, further supporting the effectiveness of this selection method.

Based on the iterative coarse-to-fine procedure, both relative VC without the reference DSM and absolute VC with the SRTM 30 m reference DSM are executed starting after pyramid-level-2 processing. At pyramid levels 3 and 2, the target surfaces are initially updated to be free of significant blunders and outliers by reducing search height ranges,

using a large height uncertainty (+/−40 m). This height uncertainty is defined by a coarse pyramid image resolution, stereo pair CA, and a height increment in the SETSM VLL definition. Additionally, the optimal heights derived from each stereo pair tend to be sparsely distributed due to strict matching success criteria in SETSM. Large height uncertainties, combined with sparsely distributed optimal heights, degrade the accuracy of height difference calculations between the optimal heights, causing substantial variability and divergence issues during the VC step. To resolve this problem, VC is started at pyramid level 1. The progress of the unit standard deviation, σ_0, in the WLSA at the first and last iterations of pyramid levels 1 and 0 is shown for Tile #2 and #3 in Figure 19. The initial σ_0 is generally lower than the final σ_0 due to fewer stereo pairs being involved in the adjustment, with the exception of Tile #3, where the σ_0 improves from 5.88 m to 4.79 m due to the bad quality of the initial selected stereo pairs. Large variations appear in the first iteration in level 1, as the optimal heights contain substantial vertical bias and noise, caused by unresolved RPC biases, and are sparsely distributed with respect to the updated surfaces from the previous level processing. After approximately 50 WLSA iterations, the variations stabilize as the SP_{ref} and expanded DSM_{ref} become well defined. At each level, the final σ_0 converges to average values of 4.75 m initially, 4.58 m at the final iteration for level 1 and 2.22 m initially, and 0.88 m at the final iteration for level 0. Peak values are observed along the progression trends and correspond to the sequential addition of dH observations from stereo pairs, as explained in Section 3.2.4. These peaks are gradually smoothed over subsequent iterations as the vertical biases of newly added stereo pairs are compensated for. After VC, 17 out of 112 and 25 out of 100 stereo pairs are identified as outliers and removed during the 3D KWHE step to generate PSMDSMs of Tiles #2 and #3, respectively.

Table 2. The number of SP_{final} at the coarsest and finest pyramid levels, according to the viewing geometry properties of CA, AA, BEA for all 4 tiles. The count is the number of stereo pairs, and the ratio is calculated by dividing each count by the total.

Viewing Geometry	Interval	Tile #1				Tile #2				Tile #3				Tile #4			
		Count		Ratio [%]		Count		Ratio [%]		Count		Ratio [%]		Count		Ratio [%]	
		Level		Level		Level		Level		Level		Level		Level		Level	
		3	0	3	0	3	0	3	0	3	0	3	0	3	0	3	0
CA	3–4	62	0	25.5	0.0	80	0	32.8	0.0	61	0	26.5	0.0	65	0	22.8	0.0
	4–5	54	23	22.2	23.0	61	37	25.0	33.0	68	38	29.6	38.0	78	50	27.4	38.8
	5–6	51	22	21.0	22.0	48	31	19.7	27.7	31	16	13.5	16.0	38	15	13.3	11.6
	6–7	26	13	10.7	13.0	23	14	9.4	12.5	30	15	13.0	15.0	25	11	8.8	8.5
	7–8	21	16	8.6	16.0	20	19	8.2	17.0	21	14	9.1	14.0	44	25	15.4	19.4
	8–9	16	14	6.6	14.0	6	5	2.5	4.5	9	8	3.9	8.0	15	9	5.3	7.0
	9>	13	12	5.3	12.0	6	6	2.5	5.4	10	9	4.3	9.0	20	19	7.0	14.7
	total	243	100	100	100	244	112	100	100	230	100	100	100	285	129	100	100
AA	0–10	92	46	37.9	46.0	98	52	40.2	46.4	97	40	42.2	40.0	113	51	39.6	39.5
	10–20	26	14	10.7	14.0	36	18	14.8	16.1	33	19	14.3	19.0	52	28	18.2	21.7
	20–30	36	17	14.8	17.0	25	12	10.2	10.7	30	21	13.0	21.0	34	23	11.9	17.8
	30–40	32	17	13.2	17.0	32	19	13.1	17.0	22	8	9.6	8.0	32	13	11.2	10.1
	40–50	43	6	17.7	6.0	34	6	13.9	5.4	36	9	15.7	9.0	31	11	10.9	8.5
	50–60	14	0	5.8	0.0	19	5	7.8	4.5	12	3	5.2	3.0	23	3	8.1	2.3
	total	243	100	100	100	244	112	100	100	230	100	100	100	285	129	100	100
BEA	90–89	39	16	16.0	16.0	38	11	15.6	9.8	44	20	19.1	20.0	41	23	14.4	17.8
	89–88	88	35	36.2	35.0	78	51	32.0	45.5	85	38	37.0	38.0	71	27	24.9	20.9
	88–87	61	28	25.1	28.0	63	25	25.8	22.3	60	31	26.1	31.0	70	33	24.6	25.6
	87–86	42	21	17.3	21.0	51	23	20.9	20.5	24	11	10.4	11.0	56	31	19.6	24.0
	86–85	13	0	5.3	0.0	12	2	4.9	1.8	17	0	7.4	0.0	42	14	14.7	10.9
	85–84	0	0	0.0	0.0	2	0	0.8	0.0	0	0	0.0	0.0	5	1	1.8	0.8
	total	243	100	100	100	244	112	100	100	230	100	100	100	285	129	100	100

Quality Analysis of PSMDSMs

Figure 20 shows PSMDSMs mosaicked from four 10 km by 10 km tiles with 1 km of edge overlap (i.e., buffers), each produced by four methods:

(1) Non-application of VC (No VC);

(2) Non-application of both VC and relative RPC bias adjustments (No VCRA);
(3) Relative VC without the reference DSM (Relative VC);
(4) Absolute VC with the reference DSM of the SRTM 30 m DSM (Absolute VC).

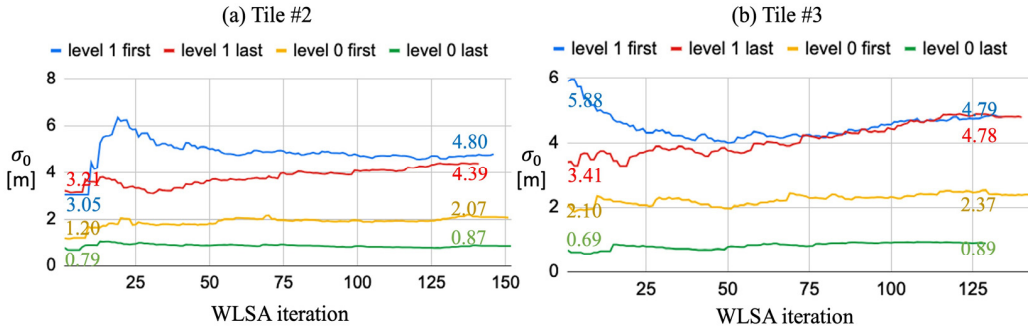


Figure 19. Plots of the standard deviation σ_0 in the Weighted Least Squares Adjustment (WLSA) fits at each processing iteration for (**a**) Tile #2 and (**b**) Tile #3. The colors indicate the first and last adjustments for the two finest coarse-to-fine pyramid levels, and the σ_0 values at each first and last iteration are labeled.

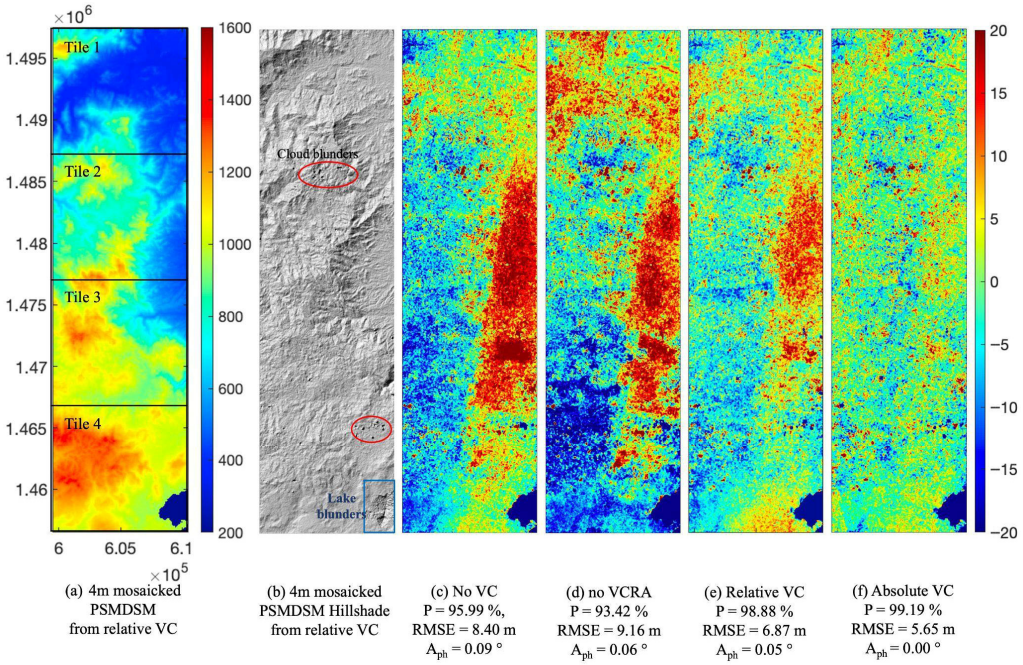


Figure 20. Height difference map comparison on the mosaicked PSMDSMs from 4 tiled DSMs generated from 1-month temporal-baseline images. Red and black circles indicate cloud blunders from PlanetScope images, respectively. Blue box located on the right bottom edge in (**b**) indicates blunders caused by lake water surfaces and masked out in the dH P and RMSE calculations.

The list of images selected for use in DSM construction is provided in Table 1. The height differences (dH) between the PSMDSM created using method 3 and WorldView3 2 m DSM exhibit far fewer blunders and outliers caused by clouds, even though many images with high fractional cloud coverage are included in the PSMDSM generation procedure, as described in Figure 20b, demonstrating the effectiveness of the relative VC method. As expected, a large lake in the southeastern end of the area of interest is a prominent area of surface noise and is masked in the dH P and RMSE calculations. Figure 20c,d show that the relative RPC bias adjustment enhances the quality of DSMs by more accurately aligning the corresponding features on the VLL and reduces the errors of vertical biases between single PSSDSMs in the SETSM MMP process, improving the percentage, P, of dH and of

RMSE within +/−20 dH from 93.42% to 95.99% and 9.16 m to 8.40 m, respectively. Adding relative VC (method 3) increases P from 95.99% to 98.88% and decreases RMSE and Aph from 8.40 m to 6.87 m and from 0.09° to 0.05°, respectively. In addition to these quantitative statistical improvements, the relative VC method dramatically minimizes the vertical biases between single PSSDSMs and enhances the quality of PSMDSMs, as shown in Figure 20e. When the reference DSM is applied in the process of VC (method 4), as shown in Figure 20f, the remaining vertical misalignment caused by vertical biases is removed, and the accuracy increases to 99.19% for P and 5.65 m for RMSE, respectively.

Figure 21 presents the quality statistics of PSMDSMs across all four tiles. When the reference DSM is applied during the VC procedure, P and RMSE range from 98.86% and 5.75 m to 99.70% and 5.31 m, respectively, with A_{ph} values of zero, confirming that the filtering process based on A_{ph} effectively eliminates PSSDSMs that have significant coordinate scaling errors. In the case of method 3 ('relative VC'), RMSE and A_{Ph} show a wider range of values, from 6.29 m and 0.00° to 7.56 m and 0.07°, than method 4 (absolute VC). This reflects sensitivity to the quality and tile coverage of SP_{ref}. Compared to method 1 (no VC), method 3 (relative VC) improves P and RMSE by an average of 2.48% and 1.53 m, respectively. In addition, to reduce vertical misalignment, as shown in Figure 20e, the incorporation of relative and absolute VC increases the proportion of dH values less than 5 m by approximately 13% and 24%, respectively, compared to the cases without VC. Further, dH values exceeding 20 m are reduced to 2.5% and 2.8%, as described in Figure 21d. Method 2 ('no VCRA') experiences the most statistical discrepancy between tile averages and the mosaicked PSMDSMs. This is primarily due to the substantial height uncertainty in buffer zones, which poorly represent the overall vertical bias of each tile.

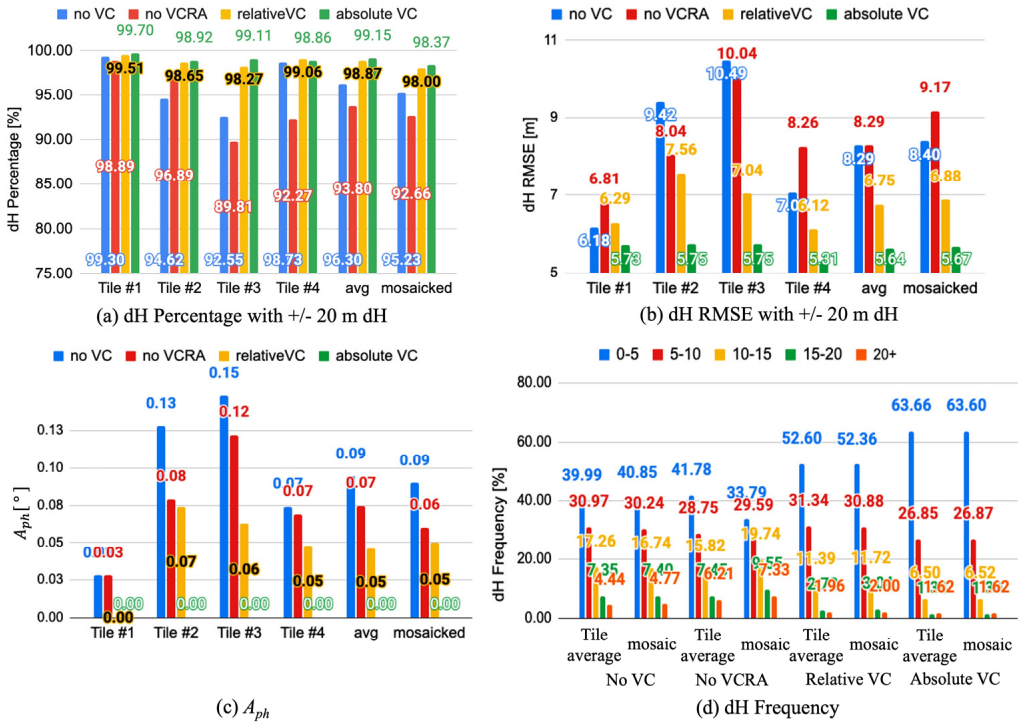


Figure 21. Quality statistics of PSMDSMs for 4 tiles and their mosaicked DSMs.

A detailed investigation of Tiles #2 and #3, which exhibit vertical misalignment on PSMDSMs due to unresolved vertical biases under method 3 (relative VC), as shown in Figure 20e, is presented using the dH map of optimal heights from SP_{ref} and the expanded DSM_{ref} at pyramid level 0, as illustrated in Figure 22. Figure 23 displays the stereo images for the SP_{ref} with 6.91° CA and 8.97° for Tiles #2 and #3, respectively. The SP_{ref} of Tile #2

covers approximately 61% of the upper-left portion of the tile, and leaves voids in the right and bottom regions of the tile, as presented in Figure 22a. These voids propagate relative VC errors when expanding the SP_{ref} coverage and generating the DSM_{ref} by unintentionally including other stereo pairs overlapping with the SP_{ref}, as illustrated in the dH map of the DSM_{ref} in Figure 22c. This error propagation is further intensified by a lack of optimal heights in the SP_{ref}, which is affected by an average cloud cover of 34% across the stereo images. The extensive cloud coverage prevents extraction of corresponding features, as shown in Figure 22a,b. The DSM_{ref} for Tile #2 is generated from six stereo pairs with CAs ranging from 7.4° to 4.5°, including three stereo pairs with Cas of less than 5°. Despite the stereo pair configuration, approximately 80% of the left region of the tile is successfully reconstructed by mitigating vertical biases and avoiding blunders due to cloud cover. The rest of the right side also demonstrates height stability. Although minor vertical errors persist throughout the DSM_{ref}, as shown in Figure 22c, and heavy clouds appear in SP_{ref}, the modified SETSM MMP approach with the proposed weight scheme effectively reduces vertical errors, surface noise, and blunders in the resulting PSMDSM. The improvement is noticeable by comparing Figures 20e and 22c. Similar patterns are observed in Tile #3. SP_{ref} of Tile #3 is derived from images with an average cloud coverage of 41% and produces data voids in the upper region. The DSM_{ref} of Tile #3 partially involves large vertical errors in the top regions, and the most clouded areas are successfully filled using optimal heights derived from overlapping stereo pairs, as shown in Figure 22g. The DSM_{ref} of Tile #3 is expanded with seven stereo pairs with CAs ranging from 10.8° to 4.7°. Except for the heavily clouded area in the middle-right portion of the tile, the PSMDSM for Tile #3 has fewer vertical errors and a better overall quality than Tile #2. This improvement is attributed to broader tile coverage of SP_{ref}, a wider SP_{ref} CA of 8.97°, and a 7% increase in the proportion of stereo pairs with a CA more than 6°. This validates the robustness and adaptability of the proposed PSMDSM generation methodology, particularly in minimizing the effects of cloud-induced blunders and surface noise.

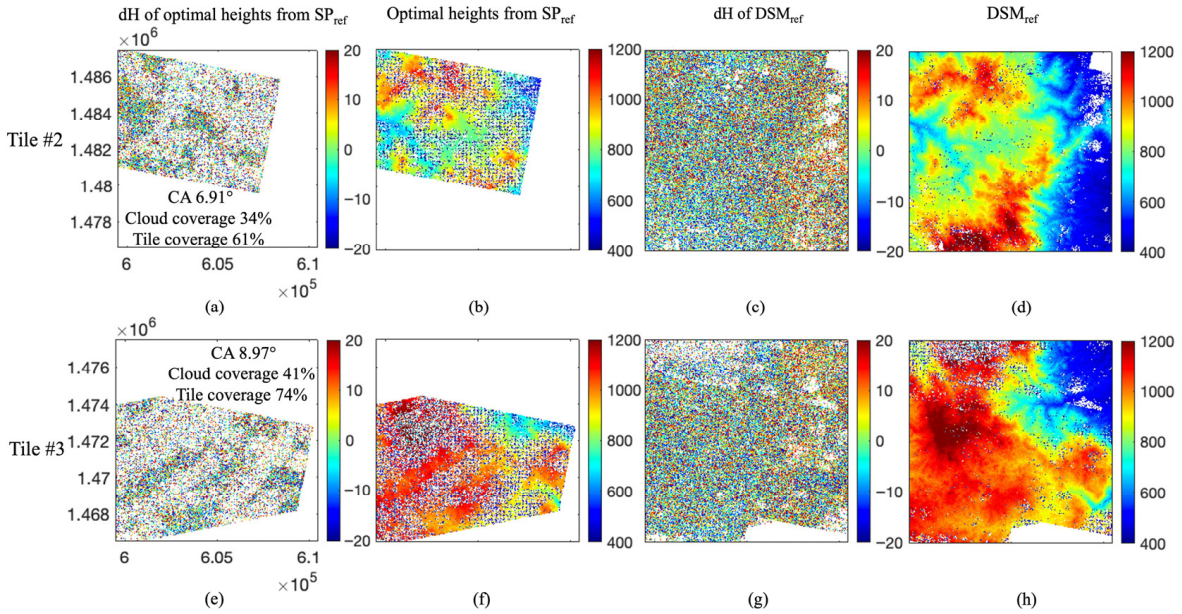


Figure 22. dH and optimal heights of SP_{ref} and DSM_{ref} for Tiles #2 and #3 (**a**–**h**). CAs of the expanded stereo pairs of SP_{ref} to generate DSM_{ref} range from 7.4° to 4.5° for Tile #2 and 10.8° to 4.7° for Tile #3, respectively.

Since the accuracy of method 3 (relative VC) is significantly influenced by the tile coverage of SP_{ref} and its expanded DSM_{ref}, we test the use of a smaller tile size of 5 km by

5 km to generate PSMDSMs for Tiles #2 and #3. A smaller tile size reduces scaling distortion issues and vertical bias errors because the DSM_{ref} can be constructed from fewer groups of overlapping stereo pairs compared to the 10 km tile size. In some cases, a single stereo pair is sufficient for use as DSM_{ref}, bypassing the reference DSM construction step. The corresponding dH maps of the 5 km tiled PSMDSMs, which are processed with method 3 (relative VC), are presented in Figure 24. The average values of P and RMSE for the four tiles are 99.51% and 5.97 m for Tile #2 and 98.70% and 5.53 m for Tile #3. Compared to the quality statistics for 10 km tile PSMDSMs, the P and RMSE are improved to 2.66% and 1.59 m for Tile #2, and 0.43% and 1.51 m for Tile #3, respectively. The dH P and RMSE of the 5 km tiled PSMDSMs are close to the results of method 4 (absolute VC). Additionally, the substantial vertical misalignment observed in 10 km tiled PSMDSMs is notably reduced with a smaller tile size, as illustrated in Figure 24. Even though the reduced tile size enhances overall DSM quality, vertical bias propagation errors and scaling issues persist, primarily due to incomplete tile coverage of SP_{ref}, high fractional cloud cover in stereo images, and characteristics of A_{ph} with better performance from method 4 (absolute VC), as shown in Figure 24b,d,f.

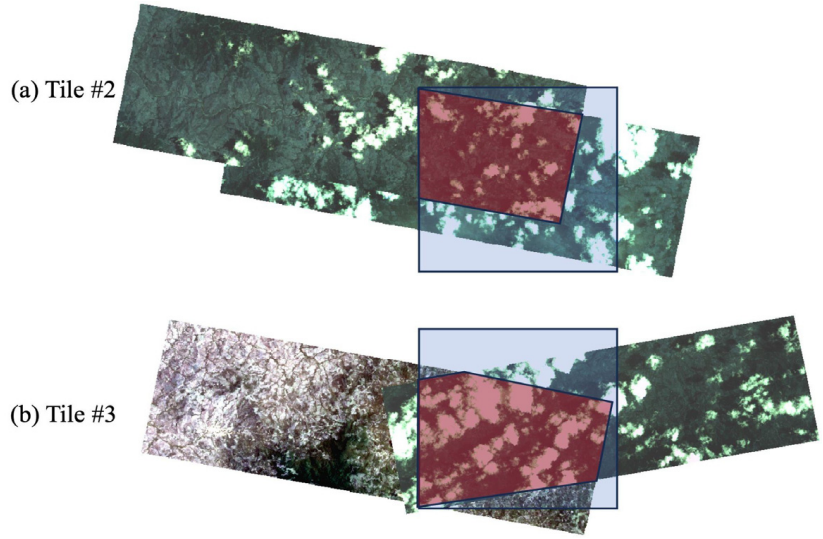


Figure 23. Stereo images and their overlap with SP_{ref} for Tiles #2 and #3. The transparent blue and red rectangles indicate the tile boundaries and the overlapped area between stereo images, respectively.

Figure 25 describes the relationship between the integrated weights of *IWHq* and the corresponding height differences, dH. *IWHq* values represent the confidence level of the estimated optimal heights derived from multiple stereo pairs and are applied to weight each optimal height during the 2D kernel-based processing step in the 3D KWHE algorithm. In the method 1 (no VC) approach, which does not reduce vertical biases or apply the scaling error filtering based on A_{ph}, the scatter plot between *IWHq* and dH shows a broader spread along the dH axis compared to the 'relative VC' and 'absolute VC' approaches. When VC is applied, vertical variances are reduced as shown in Figure 25c, leading to an improved correspondence that more accurately reflects the achievable accuracy associated with each *IWHq* value. Furthermore, positions with low *IWHq* values correspond well to positions with large dH values in the dH map. Using method 4 (absolute VC), more stereo pairs are filtered out using A_{ph} estimated from the reference DSM compared to method 3. As a result, the *IWHq* values in method 4 are generally lower than those in method 3, reflecting the improved filtering.

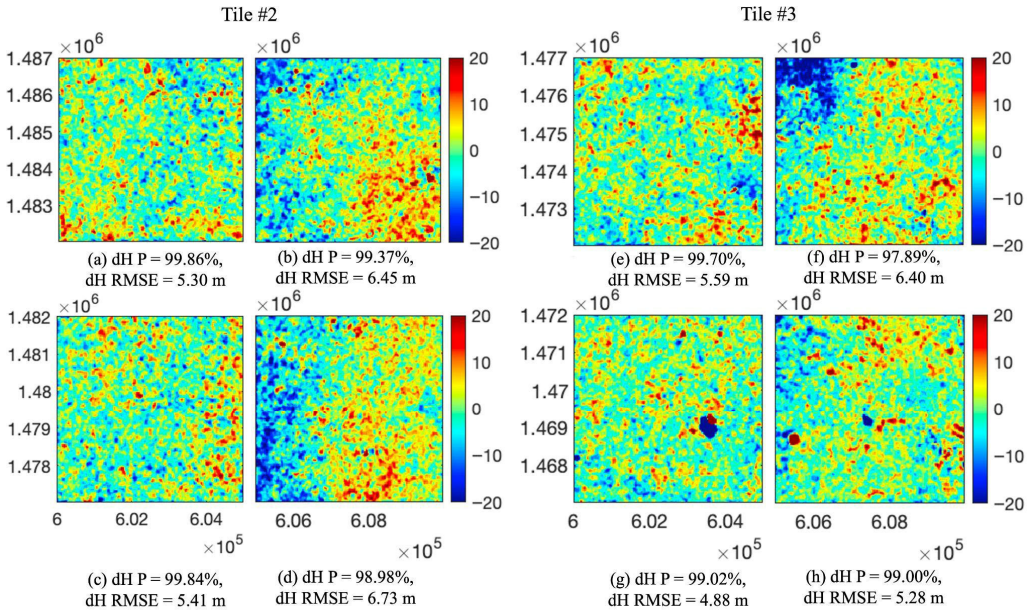


Figure 24. dH P and RMSE statistics of PSMDSM tiled by 5 km by 5 km for Tiles #2 and #3.

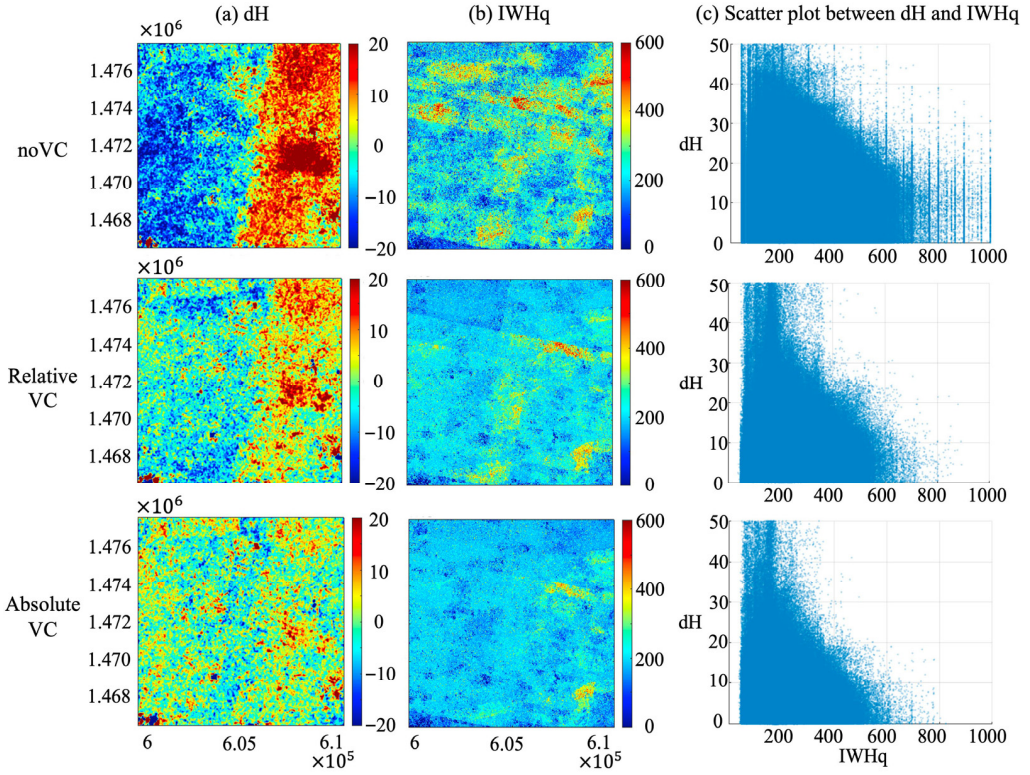


Figure 25. Color scale maps of Tile #3 (**a**) dH and (**b**) *IWHq* and (**c**) scatter plots showing the pixel-by-pixel relationship between the map values for the cases of (**top row**) no VC, (**middle row**) relative VC, and (**bottom row**) absolute VC.

4.1.4. PSMDSMs with Increased Image Temporal Baseline

To assess the impact of increasing the temporal baseline between images, the number of SP_{final} and associated images are automatically and iteratively determined by the optimized stereo pair selection procedure for generating PSMDSMs using a 4-month maximum temporal baseline from 1 March to 30 June. The number of stereo pairs and images at pyramid level 0 ranges from 125 to 100, from 46 to 36 for the four tiles, respectively, or approximately twice the number when using a 30-day baseline. Figure 26 presents the

resulting, mosaicked PSMDSMs, using the same method categories shown in Figure 20. With the extended temporal baseline, stereo pairs with fewer clouds and larger tile coverage are selected, resulting in blunder-free PSMDSMs, as illustrated in Figure 26b. Additionally, vertical misalignment in the dH maps is notably reduced across all methods when compared to Figure 20. In the method 4 (absolute VC) approach, quality statistics of dH P and RMSE are slightly improved to 99.67% and 5.16 m, respectively, from 99.19% and 5.65 m in the 1-month PSMDSMs, effectively removing blunders caused by cloud cover and reducing surface noise. Although the 'no VC' and 'no VCRA' approaches still exhibit considerable vertical errors, as seen in Figure 26c,d, their quality statistics are improved, with dH P increased by approximately 2.3% and dH RMSE decreased by about 1.6 m. For the 'relative VC' approach, Figure 27 compares quality statistics between PSMDSMs generated with 1-month and 4-month temporal baselines. Tile #3 shows the most significant improvement, with dH P increased from 98.27% to 99.68% and dH RMSE decreased from 7.04 m to 5.48 m. Across all 4 tiles, the average dH RMSE is improved by 17%, consistent with the improvements observed in the mosaicked PSMDSM. These results demonstrate that PSMDSM quality can be enhanced by incorporating a broader set of available images, providing more stereo pairs with a broader range of viewing geometries. The proposed methodology not only supports automated cloud blunder mitigation but also improves overall PSMDSM quality by iteratively selecting well-defined stereo pairs. Figure 28 presents a DSM hillshade comparison of selected subregions between the SRTM (30 m resolution), SETSM WorldView (2 m) and PSMDSMs (4 m) with a 4-month temporal baseline. PSMDSMs resolve terrain features at a level of detail comparable to the SETSM WorldView DSM despite having half the pixel resolution, while reducing the surface noise. This demonstrates that tiled PSMDSMs have the potential to provide a global elevation dataset that surpasses SRTM and other available DSMs in terms of geomorphological representation, provided that vertical biases are properly mitigated using either a reference DSM or carefully selected SP_{ref}.

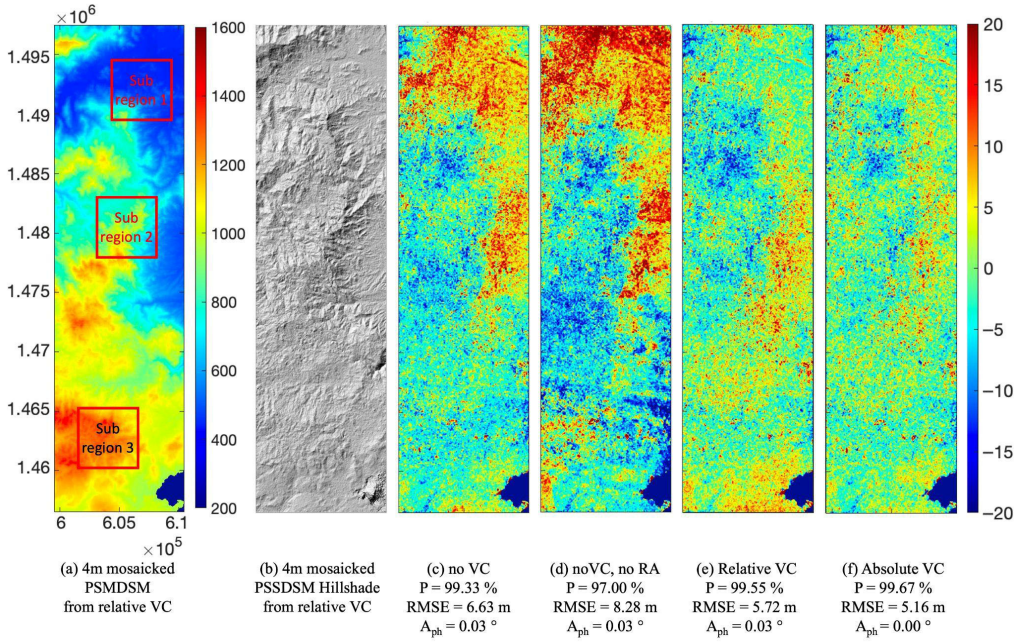


Figure 26. Comparisons on the mosaicked PSMDSMs from 4 tiled DSMs generated from 4-month temporal-baseline images.

Figure 29 shows a comparison of quality statistics based on combinations of CAs and image cloud coverage. PSMDSM quality may improve with a greater number of stereo pairs with wider CAs. Holding the maximum cloud coverage constant at 50%,

Figure 29 compares dH P and RMSE of PSMDSMs generated using stereo pairs with 'CA > 3', 'CA > 6', and 'CA > 8'. The 'CA > 6' and 'CA > 8' cases show degraded overall quality, with a 10% lower P and 2 m greater RMSE compared to 'CA > 3'. This deterioration is due to the inclusion of high fractional cloud cover images, which fail to reconstruct the full tile area without blunders, as shown in Figure 30b,c. To mitigate cloud-induced blunders, PSMDSMs are also generated using stereo pairs with less than 10% and 30% cloud coverage, while maintaining CA at 3°. The 'Cloud < 30' case results in similar statistics to the 'Cloud < 50' case. However, the 'Cloud < 10' case presents the lowest dH P at 76.27%, despite reducing blunders compared to Figure 30b, due to excessive filtering of stereo pairs that results in significant void areas across the tiles. These results demonstrate that the proposed methodology effectively produces high-quality PSMDSMs by minimizing the impact caused by low-quality images and poor stereo geometry, even under relaxed stereo pair selection criteria.

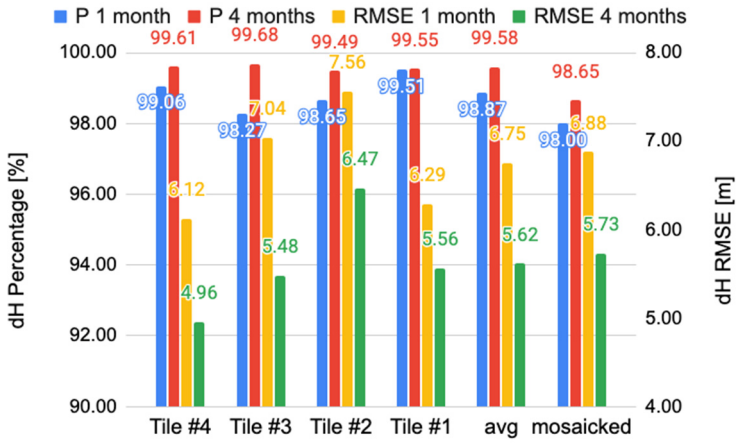


Figure 27. Comparison of quality statistics between PSMDSMs generated with 1-month and 4-month temporal baselines.

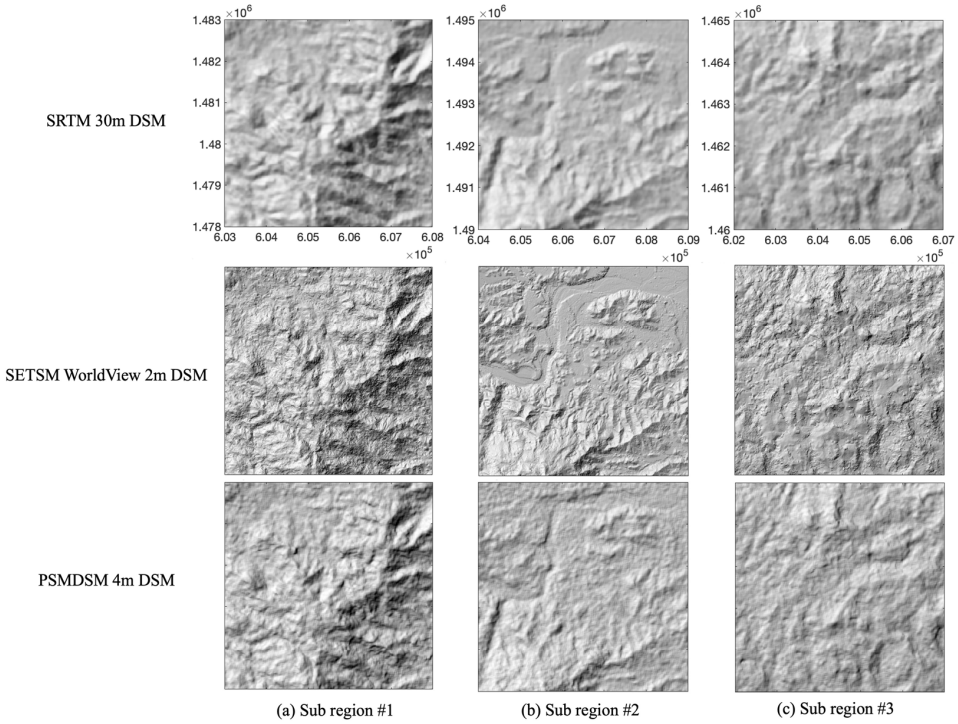


Figure 28. DSM hillshade comparison over the subregions between SRTM 30 m, SETSM WorldView 2 m and PlanetScope Dove 4 m DSM with a 4-month temporal baseline.

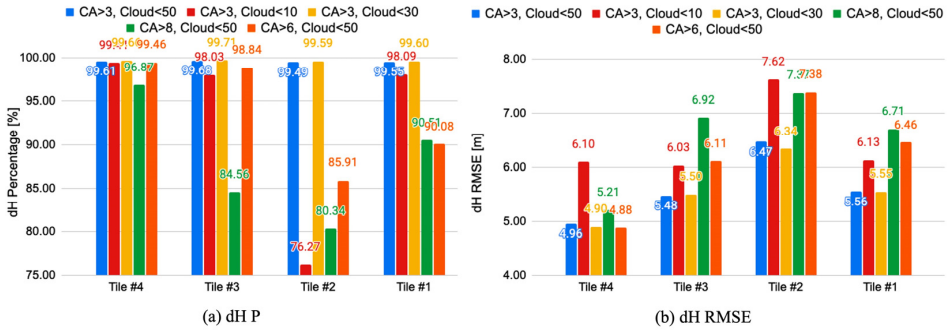


Figure 29. Quality statistics comparison according to CA and cloud coverage.

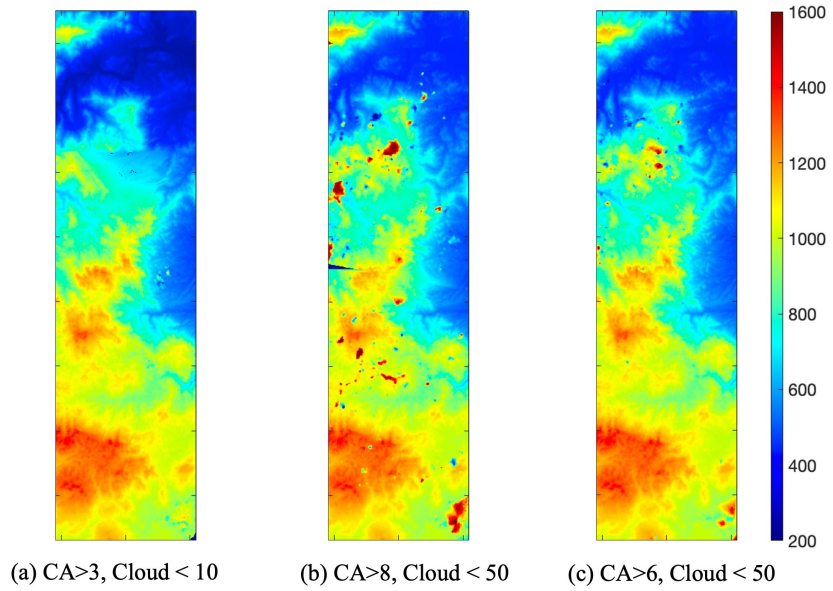


Figure 30. Mosaicked PSMDEMs from the 4 tiles with various combinations of CA and cloud coverage.

4.1.5. Analysis of Seamless PSMDSM Mosaic for Pantasma Crater Region

A total 568 images are utilized to generate PSMDSMs over a 70 km by 60 km area, as shown in Figure 14a. The methods of 1 (no VC), 3 (relative VC), and 4 (absolute VC) are applied to evaluate DSM quality, and tile sizes of 10 km and 5 km are tested to analyze the dependency of quality on tile size, as presented in Figure 31. Adjacent tiles overlap by 10% for mosaicking. The mosaicked PSMDSMs show reduced accuracy compared to individual PSSDSMs due to merging errors at four overlapped buffer boundaries, leading to misestimation of overall vertical biases for individual tiles due to different attributes of each SP_{ref} and DSM_{ref}. As a result, the mosaicked 10 km tiled PSMDSMs produce similar quality in the 'No VC' and 'relative VC' cases, with dH P and RMSE of 86.13% and 8.42 m for 'No VC', and 84.10% and 8.94 m for 'relative VC', respectively, although vertical biases are effectively minimized within each tile, as shown in Figure 26e, and quality statistics for individual tiles are improved, as shown in Figure 32. The merging errors are more pronounced in the mosaicked 5 km tiled PSMDSMs, where dH RMSE increases to 9.31 m from 8.94 m obtained for the 10 km tile due to an increasing number of varied SP_{ref} and DSM_{ref} contributing to inconsistencies, while individual tile quality is improved with the smaller tiles, as shown in Figure 32. The average dH P and RMSE for 5 m tiled PSMDSMs are improved from 92.43% to 95.64% and 7.00 m to 6.16 m, respectively, compared to the 10 km tiled PSMDSMs. The average values reach the accuracy level of the 'absolute VC'. Some 10 km tiled PSMDSMs fail to produce DSM_{ref} due to the filtering of stereo pairs with distorted coordinates, which occurs due to the scaling issue described in Section 3.2.2, and a high fraction of heavily clouded images, resulting in voids. In contrast, all PSMDSMs

created in 5 km tiles successfully produce complete DSMs due to benefits from broader SP_{ref} coverage and higher A_{ph} accuracy in stereo pairs. Even though the quality statistics differ between 'relative VC' and 'absolute VC' (methods 3 and 4), the hillshade images present similar surface feature representations and comparable levels of cloud-induced blunders. The 'absolute VC' method (method 4) resolved most vertical errors using one reference DSM for DSM_{ref} generation.

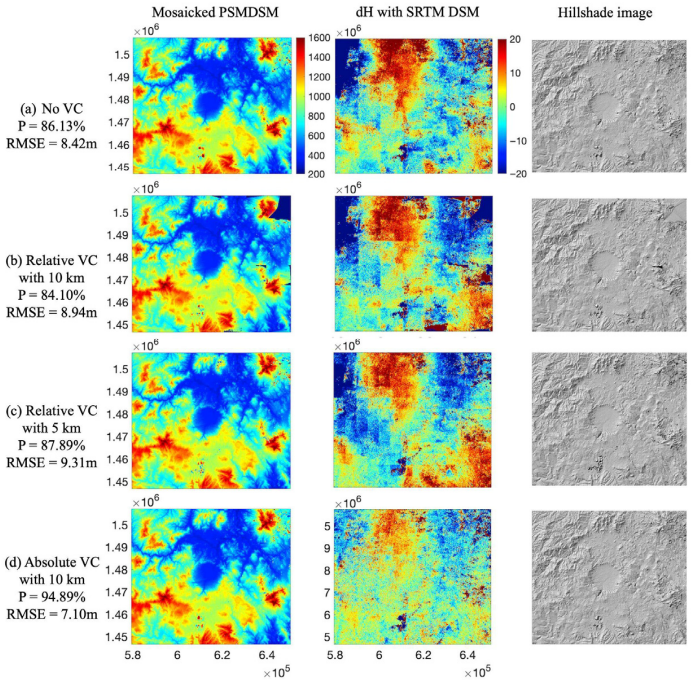


Figure 31. Mosaicked PSMDEMs for 70 km by 60 km target region according to three VC applications of 'No VC', 'relative VC', and 'absolute VC', and difference tile sizes of 10 km and 5 km.

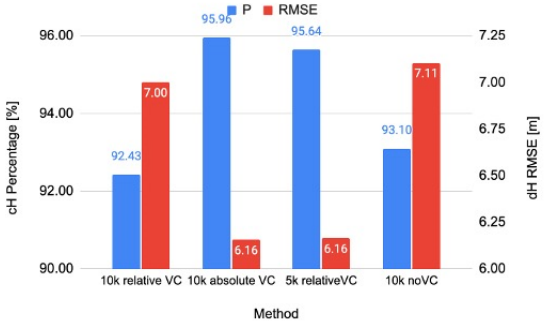


Figure 32. Mean statistics of dH P and RMSE for different methods, and correlation plots between dH RMSE and height range over 70 km by 60 km target region.

To analyze a possible dependence of accuracy on target height range, CA, AA, and BEA, scatter plots for PSMDSMs generated using the 'relative VC' method (method 3) with tile sizes of 5 km and 10 km are presented in Figure 33. Both of the tile size cases reveal a strong correlation between dH RMSE and terrain height range, as illustrated in Figure 33a,b, compared to weaker correlations with CA, AA, and BEA in the other scatter plots. The dH RMSEs of individual PSMDSMs range from 3.32 m to 10.24 m for 5 km tiles and from 4.27 m to 10.56 m for 10 km tiles. All values of dH RMSE versus height range in Figure 33a,b fall within parallelograms with a width of 5.8 m and a slope of 172.4 for 5 km tiles and a narrower width of 4.8 m and a steeper slope of 285.7 for 10 km tiles. The change in slope reflects the tile size, with the 10 km case exhibiting a smaller variation in dH RMSE across different height ranges than the 5 km case. At the same height range, the

dH RMSE for 10 km tiles can be estimated more precisely due to the narrower width of the parallelogram, despite the higher absolute RMSE values. This analysis suggests that the minimum and maximum achievable accuracy of PSMDSMs at a given height range can be predicted by the parallelogram's width. In addition, a large height range significantly degrades PSMDSM quality due to scaling errors, particularly in stereo pairs with narrow convergence angles. These errors are not captured by the A_{ph} value of the fitted 3D plane, because they are not directly predictable by viewing geometry alone. Figure 34 shows an example PSMDSM that suffers from severe scale errors with a large height range. As a result, Figure 31 shows numerous vertical errors seen in individual PSMDSMs. The dH RMSE of PSMDSMs shows weak correlation with CA, AA, and BEA, as indicated by the sparse scatter plot distribution. The 'CA > 7' case for 5 m tiles shows a similar correlation of PSSDSMs as explained in Section 4.1.2 with Figure 16d. However, for the 'AA < 10°' case, the strong correlation with PSSDSMs, as found in Figure 16a, is not evident due to the influence of the weighted multiple-pair matching process applied in PSMDSM generation. The 'BEA > 88' case shows a general trend of improved dH RMSE, corresponding to an increased number of stereo pairs with BEAs more than 88°.

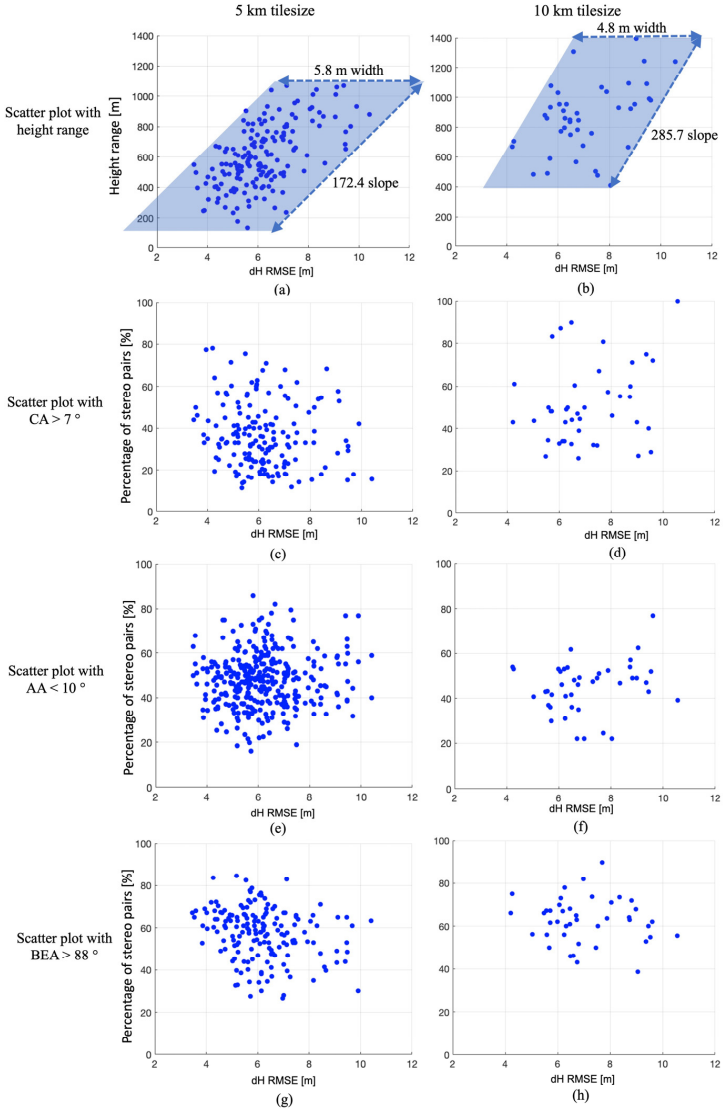


Figure 33. dH RMSE scatter plot with height range, stereo pairs with a more than 7° CA, less than 10° AA (AA10), and more than 88° BEA for 5 km and 10 km tiled PSMDSMs (**a**–**h**). The percentage of stereo pairs is calculated by dividing the number of stereo pairs for the corresponding conditions by the number of SP_{final}.

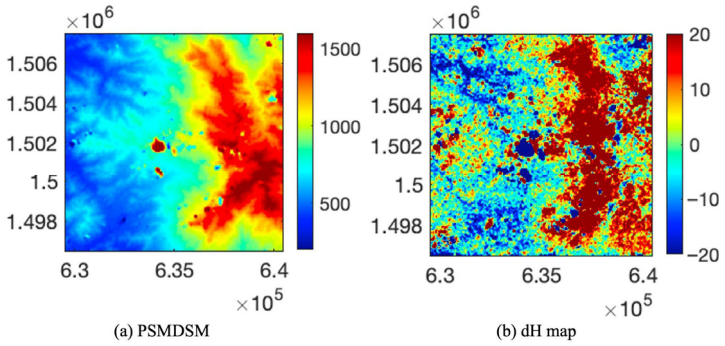


Figure 34. A PSMDSM impacted by severe scaling errors due to a large range in surface heights (i.e., high relief). The height range calculated by SRTM 30 m DSM is 1394 m, and dH P and RMSE for this DSM are 79.20% and 9.05 m, respectively.

4.2. Other Impact Craters

To demonstrate the adaptability and practicality of the proposed automated DSM generation methodology, PSMDSMs are also generated for four additional impact craters located in Libya, Kazakhstan and Bolivia with a variety of image textures. Tile boundaries for these craters are defined based on the UTM projection. Table 3 summarizes the quality statistics of the PSMDSMs for each crater. The height ranges for all craters are less than 300 m, which minimizes scale errors and results in more accurate PSMDSMs compared to the Pantasma case. The PSMDSMs with 4 m grid spacing are generated without tiling, and height differences are calculated against SRTM 30 m DSMs acquired on 11 February 2000. For method 4 (absolute VC), SRTM DSMs are used as reference DSMs. The resulting dH RMSEs range from 3.71 m to 5.77 m for the 'relative VC' method, and from 2.87 m to 5.62 m for the 'absolute VC' method. The statistics align well with the correlation between dH RMSE and a height range below 300 m, as described in Figure 33.

Table 3. PSMDSM quality statistics for Oasis, British Petroleum Structure, Bigach, and Iturralde craters.

Crater Name	Country	Location		Temporal Baseline [Day]	Tile Size [km]	Height Range [m]	Quality Statistics from dH			
							Relative VC		Absolute VC	
		Latitude	Longitude				P [%]	RMSE [m]	P [%]	RMSE [m]
Oasis	Libya	24.57N	24.43E	30	8	138.83	96.67	5.77	96.93	5.63
British Petroleum Structure	Libya	25.35N	24.32E	30	4	106.45	95.64	5.59	95.58	5.62
Bigach	Kazakhstan	48.52N	82.01E	60	15	277.21	100.00	3.71	100.00	3.73
Iturralde	Bolivia	12.75S	64.71W	90	10	47.09	99.98	4.36	100	2.87

4.2.1. Oasis Crater in Libya

For the 8 km by 8 km Oasis crater region, a total of 164 images are collected from the PlanetScope API within a 30-day temporal baseline starting on 1 May 2020. A PSMDSM is generated using 40 automatically selected images from 96 candidate images, with 66% of the stereo pairs having more than 9° Cas, as shown in Figure 35e. The Oasis crater is surrounded by desert terrain, as presented in Figure 35a, which is subject to rapid changes due to wind and other weather conditions. The selected images have severe saturation, which causes discrepancies in radiometric information between images of the same surfaces, as illustrated in Figure 35d. Despite challenges posed by surface variability and radiometric inconsistencies, the generated PSMDSM accurately reconstructs the morphological features of the crater, including its shapes and elevation, as demonstrated in Figure 36. The height profile along the line P1 over crater surfaces shows comparable or improved spatial resolution relative to the SRTM 30 m DSM, as presented in Figure 36d. However, numerous blunders over the desert terrain remain on the DSM due to challenging surface properties,

which reduce the dH P to below 97% and increase the dH RMSE to above 5 m. The quality statistics between the 'relative VC' and 'absolute VC' are nearly identical, with a difference of less than 0.3% in dH P and 0.15 m in dH RMSE.

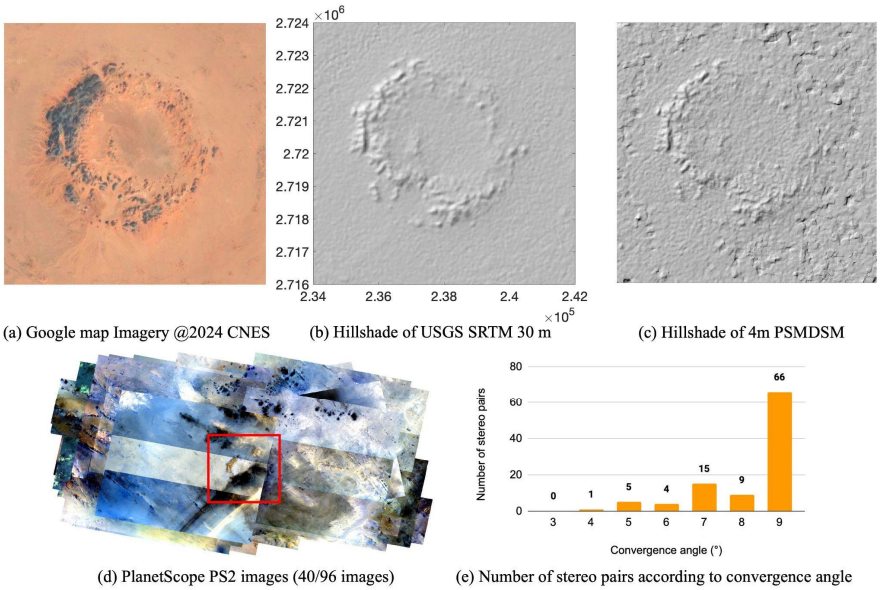


Figure 35. Hillshade images of SRTM 30 m DSM (**b**) and a PSMDSM (**c**) for the Oasis crater with used PlanetScope PS2 images (**d**). The red box indicates the tile boundary of the PSMDSM.

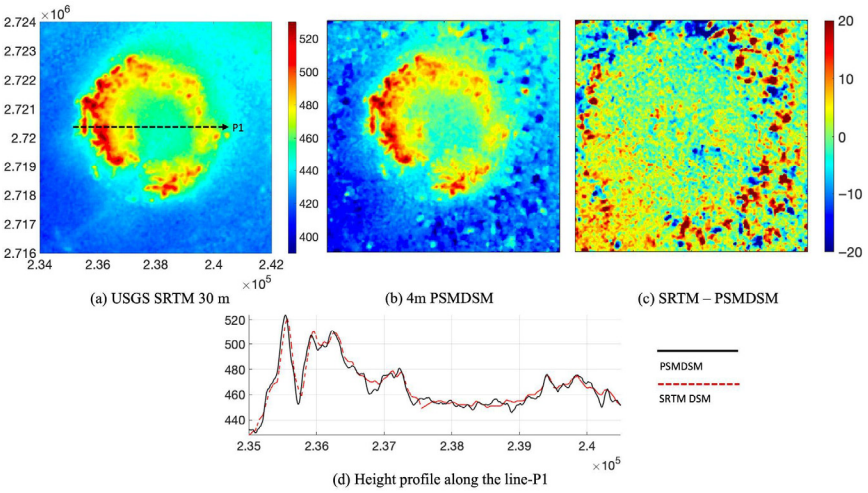


Figure 36. SRTM 30 m DSM and a PSMDSM for the Oasis crater.

4.2.2. British Petroleum (B. P.) Structure Crater in Libya

Using the same temporal baseline as the Oasis crater over a 4 km by 4 km square centered on the B.P. Structure crater region, a PSMDSM is generated using 31 images, forming 44 stereo pairs with a CA greater than 9° and a total of 75 stereo pairs with a CA exceeding 6°, as shown in Figure 37e. Similar to the Oasis crater, the B. P. Structure cater is in desert terrain. The increased proportion of wide CA stereo pairs effectively reduces low-magnitude surface noise. However, the challenging surface properties and radiometric inconsistencies result in high-magnitude height blunders, as presented in Figures 37c and 38c. These blunders result in a decrease of approximately 1% in the dH P compared to the Oasis crater case. The height profile along line P2 presents a good match in crater rim elevation between SRTM and PSMDSM; however, mismatches remain over desert surfaces due to the blunders, as shown in Figure 38d. The quality statistics between the two VC methods are comparable to those observed for the Oasis crater case.

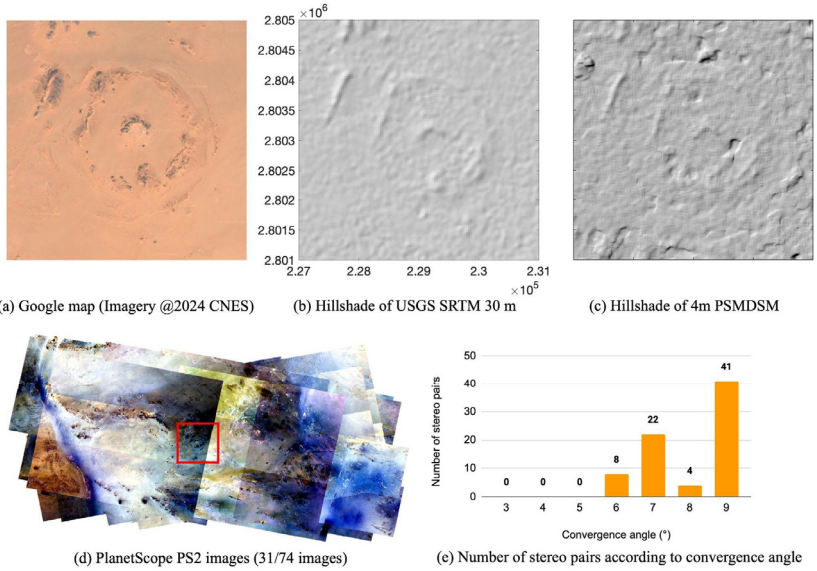


Figure 37. Hillshade images of SRTM 30 m DSM (**b**) and a PSMDSM (**c**) for the B.P. Structure crater with used PlanetScope PS2 images (**d**). The red box indicates the tile boundary of the PSMDSM.

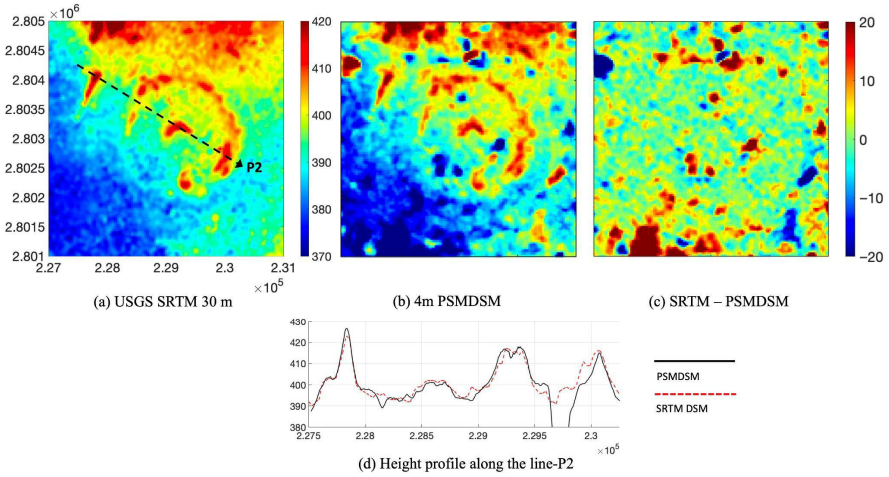


Figure 38. SRTM 30 m DSM and a PSMDSM for the B.P. Structure crater.

4.2.3. Bigach Crater in Kazakhstan

With the Bigach crater measuring approximately 9 km in diameter, a 15 km by 15 km target region centered on the crater is defined for PSMDSM generation. The 15 km tile size can be applied because the height range of 277 m is substantially narrower than that of the Pantasma test site. A total of 513 candidate images are collected within a 60-day temporal baseline starting on 1 May 2020. A total of 115 images are automatically selected by the proposed optimized stereo pair selection step to generate the PSMDSM, with 76% of the stereo pairs having a more than 7° CA, as shown in Figure 39e. The Bigach crater is surrounded by vegetated surfaces with a height range of 277 m, as presented in Figure 39a. Many of the selected images contain heavily clouded textures, as shown in Figure 39d. Despite the heavily clouded images, the generated PSMDSM accurately captures the topographical features of mountain ridges and crater rims without significant blunders. In addition, finer-scale surface undulations are more observable compared to the SRTM DSM, as illustrated in Figure 40d. The height difference map in Figure 40c reveals low-magnitude surface noise, primarily attributed to forest cover and the finer spatial resolution of the PSMDSM. The overall accuracy of PSMDSM in terms of dH RMSE is within 3.75 m for both methods 3 (relative VC) and 4 (absolute VC), with a dH P of 100%.

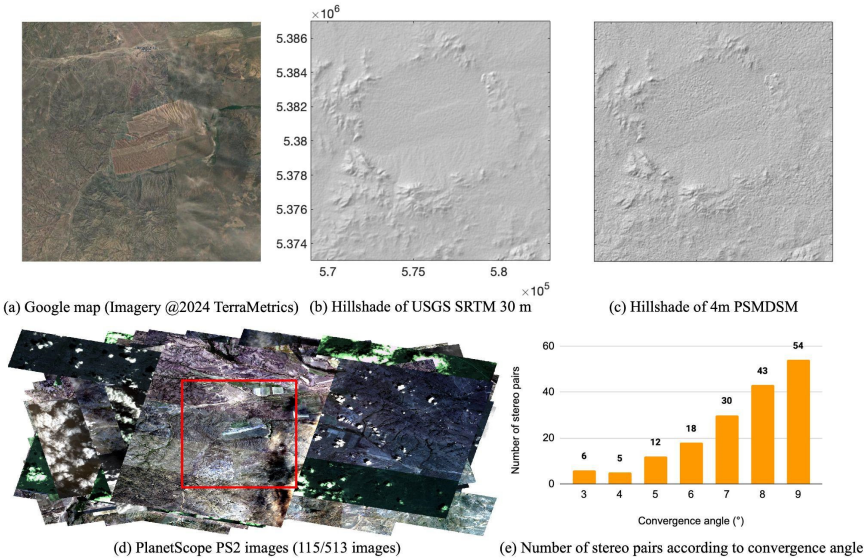


Figure 39. Hillshade images of SRTM 30 m DSM (**b**) and a PSMDSM (**c**) for the Bigach crater with used PlanetScope PS2 images (**d**). The red box indicates the tile boundary of the PSMDSM.

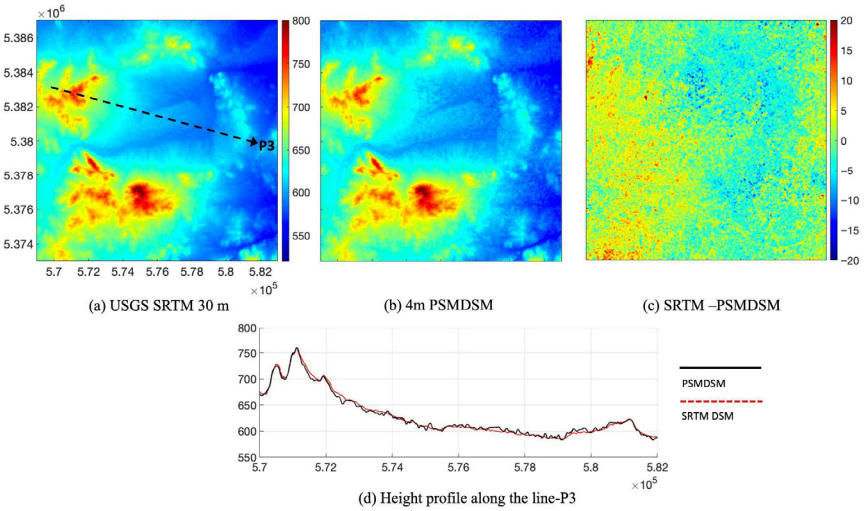


Figure 40. SRTM 30 m DSM and a PSMDSM for the Bigach crater.

4.2.4. Iturralde Crater in Bolivia

The 10 km by 10 km target region is defined for PSMDSM generation based on the approximately 8 km diameter of the Iturralde crater. A total of 90 candidate images are collected within a 60-day temporal baseline starting on 1 June 2020. The PSMDSM is generated using 41 selected images from the 90 candidate images. A total of 98 stereo pairs are configured, with 63 stereo pairs with greater than 8° CAs, as shown in Figure 41e. The Iturralde crater is relatively flat, with a height range of 47 m, and is primarily covered by forests and marshland. The bottom right region, which covers approximately 25% of the tile area, is dominated by marshland, as shown in Figure 41a. These marsh textures introduce significant height variation during the image-matching process, especially compared to forested areas, resulting in notable vertical errors in the vertical coregistration procedure. As a result, the PSMDSM generated from the 'relative VC' approach shows visible vertical errors at the bottom of the crater, as shown in Figure 42c. The vertical errors are effectively mitigated by the 'absolute VC' using the SRTM DSM as a reference. Surface changes are observed both inside and outside the crater rims due to variations in forest and marsh conditions, as reflected in the 'absolute VC' results and the height profile along line P4 in Figure 42e. While the spatial pattern of changes is consistent between both VC methods, the

dH RMSE from the 'relative VC' approach is 1.5 m higher than the 2.87 m RMSE obtained from the 'absolute VC'.

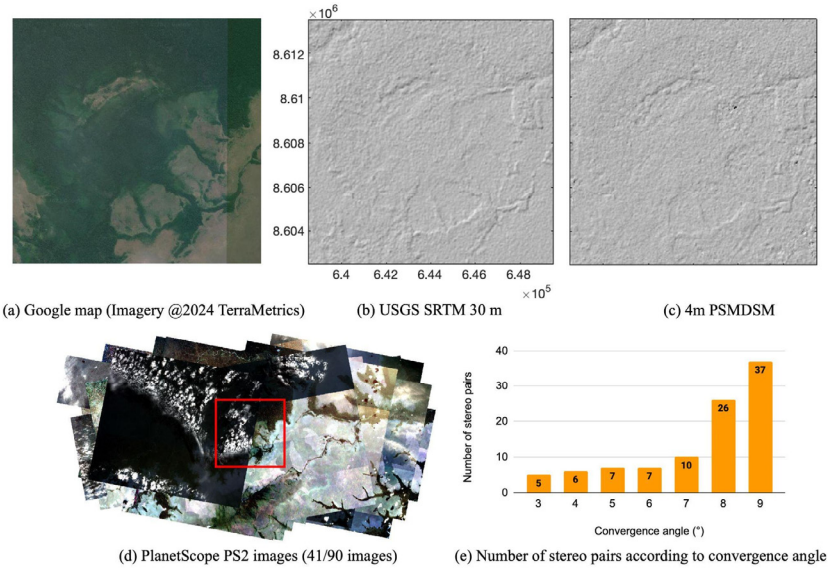


Figure 41. Hillshade images of SRTM 30 m DSM (**b**) and a PSMDSM (**c**) for the Iturralde crater with used PlanetScope PS2 images (**d**). The red box indicates the tile boundary of the PSMDSM.

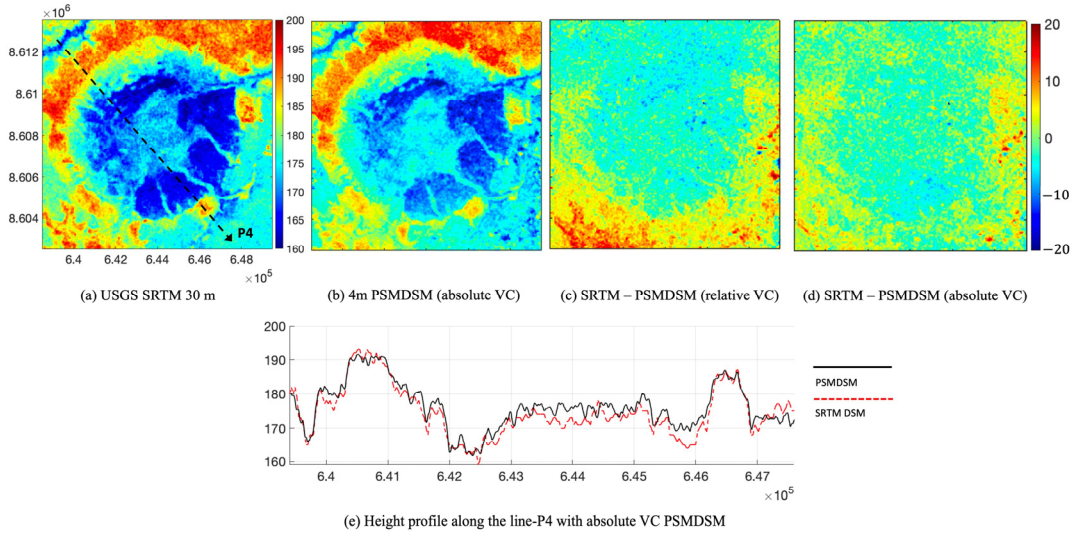


Figure 42. SRTM 30 m DSM and a PSMDSM for the Iturralde crater.

5. Discussion

PlanetScope PS2 images are primarily designed for Earth monitoring and are captured with near-nadir viewing geometry, featuring tilt angles of less than 5°. To retrieve surface elevation information from the images, a multiple-image-matching technique is essential to reduce the large height uncertainty in single stereo pairs with such narrow convergence angles. The quality of optical stereophotogrammetric DSM generation is also significantly affected by image texture issues such as cloud cover and radiometric instabilities, including saturation, that are common in our test datasets for impact craters in a range of environments. In areas with extensive cloud cover, such as the subtropical Pantasma crater in Nicaragua, our proposed image selection methodology effectively eliminates the need for time-consuming manual interpretation by introducing an optimized stereo pair selection method and enables fully automated DSM generation from PlanetScope PS2 imagery. This method initially identifies well-defined stereo pairs based on three conditions: geomet-

ric suitability, texture quality, and mapping completeness. To finalize the selection and optimize computational loads without DSM quality loss, a Weighted Stereo Pair Index (WSPI) is developed, which ranks stereo pairs by integrating three stereo pair viewing geometric parameters, asymmetric angle, bisector elevation angle, and convergence angle, and one mapping criterion, matching success ratio. The WSPI is experimentally derived through the quality analysis of PSSDSMs, which demonstrates a strong correlation between PSSDSM accuracy and the geometric parameters of CA, AA, and BEA. The experimental results confirm that the optimized stereo pair selection method effectively reduces the number of required stereo pairs for DSM generation, ensuring compatibility with available computational resources, increasing the number of stereo pairs with well-defined stereo viewing geometry, and completely covering the targeted tile region without voids.

Without RPC corrections obtained from bundle adjustment of ground control points (GCPs), positional discrepancies between the extracted optimal heights from individual stereo pairs are inevitable and primarily introduce vertical errors during the process of merging multiple stereo pair DSMs. The vertical and scaling errors are amplified in PlanetScope PS2 stereo pairs due to their extremely narrow convergence angles, which causes greater height uncertainty compared to conventional satellite imagery. To mitigate these errors without relying on GCPs or a reference DSM, a novel inter-plane vertical coregistration (VC) method is developed. This method iteratively constructs reference surfaces by expanding the coverage of a selected reference stereo pair. The proposed relative VC technique effectively addresses scale distortion, which is quantified by the horizontal angle (A_{ph}) of the 3D height difference plane. The approach applies reference surfaces using reference weights (W_{ref}), derived by incorporating the viewing geometry parameters of CA, AA, and BEA, as well as image-matching quality of NCCs, and the average of all pairwise A_{ph} values, which represents surface stability. Vertical biases between stereo pairs are sequentially estimated using these reference surfaces, and PSMDSMs are generated through the SETSM 3D KWHE procedure with the proposed weighting scheme. Compared to tiled PSMDSMs generated without the 'relative VC' and relative RPC bias adjustment, the relative VC method significantly reduces vertical errors, improving dH and RMSE up to approximately 10% and 43%, respectively, and increasing the proportion of grid cells within the '0 to 5 m' dH range by up to 26%. When applying an external DSM, such as an SRTM DSM, as the reference surfaces, as termed by 'absolute VC', vertical errors in relative VC-based PSMDSMs are further minimized since the SRTM DSM is free of the scaling issue and completely covers the target tile regions, resulting in the highest quality of PSMDSMs, with 99% and 5 m levels of dH P and RMSE. The quality of PSMDSMs using the 'relative VC' approach is further enhanced by adopting a smaller tile size of 5 km compared to 10 km, which results in similar-quality PSMSDMs to results obtained using the 'absolute VC' approach by increasing the accuracy of stereo pair scaling error measurements and tile coverage of reference stereo pairs. The application of a smaller tile size can improve DSM quality by reducing the number of expanding stereo pairs required to construct reference surfaces, DSM_{ref}, or by eliminating the reference surface construction step when a well-defined single stereo pair that entirely covers the tile area is available. However, smaller tile sizes increase the processing time for large-area DSM generation by merging multiple tiled DSMs, since multiple buffer zones are repeatedly applied. Furthermore, vertical bias errors and scaling issues in the mosaicked large-area DSM can be severely affected by inconsistencies among reference stereo pairs used in adjacent tiles. The appropriate tile size should be determined based on the spatial extent of the target area and characteristics of the terrain in the absence of existing reference surfaces. In addition, extending the temporal baseline to incorporate more stereo images in the proposed PSMDSM generation procedure improves the PSMDSM quality by selecting more well-defined stereo pairs,

without introducing blunders caused by heavy cloud coverage and quality degradation from poor viewing geometry of stereo pairs.

An integrated weight function (*IWHq*) within the SETSM 3D KWHE is modified to estimate final optimal heights from multiple optimal heights to generate PSMDSMs. Large weight values enhance the potential for accuracy improvement at individual PSMDSM grid cells and limit the maximum achievable accuracy for each grid. Based on analysis of 70 km by 60 km tiled PSMDSMs, a strong proportional relationship is observed between dH RMSEs and terrain height ranges by using scatter plots. This relationship suggests that both minimum and maximum expected PSMDSM accuracy can be predicted at a certain height range, which is defined by the width of a parallelogram and the slope of its sides. Based on the parallelogram analysis, a 10 km tile size increases accuracy compared to a 5 km tile size. These analyses indicate that the most influential factors in determining PSMDSM quality are the scale-related parameters of satellite altitude and terrain elevation range. A seamless, continental-scale PSMDSM can be produced by mosaicking tiled individual PSMDSMs. Mosaicked PSMDSMs generated using the 'relative VC' method are severely affected by tile inconsistencies due to merging errors at the overlapping buffer boundaries. Although hillshade representations may appear visually consistent, these errors lead to errors in vertical bias estimation for individual tiles because each tile is based on a different reference stereo pair and expanded reference surfaces. Therefore, when PSMDSMs are utilized for surface change detection or topographical analysis in remote sensing applications, researchers must carefully consider scale errors caused by target height ranges and satellite altitude, impacts of tile size, and whether the data has been mosaicked, particularly when using the 'relative VC' approach. To further validate the robustness of the proposed automated DSM generation methodology, PSMDSMs are also generated for four additional craters, the Oasis and British Petroleum craters in the Libyan Desert, Bigach crater in Central Asia, and Ituuralde crater in Bolivia. The results from these contrasting regions demonstrate that the proposed methodology is effective at selecting the best set of available imagery to produce a seamless DSM, with the quality of the final DSM mostly dependent on the limitations of the PlanetScope image quality, such as radiometric stability and saturation, as is most clearly apparent over challenging desert and marshland surfaces. For good-quality images, PSMDSMs reconstruct detailed terrain features at 4 m grid spacing, comparable to SETSM WorldView 2 m DSM, but with the potential for global land coverage and frequent repeats for change detection and measurement, provided that vertical biases are properly mitigated. The empirically derived weights and functions were evaluated using five target crater regions, which mostly cover diverse terrain types, including flat, mountainous, vegetated, and desert surfaces, with surface elevation ranges of up to 1400 m. These approaches were implemented within a fully automated framework and demonstrated improved performance, as described in Section 4. These values may require further tuning to achieve optimal performance and are particularly sensitive to the geometric distribution of the CA, AA, and BEA in stereo pairs, which determines the relationship between DSM accuracy and geometric configuration. In addition, terrain types such as urban areas, which were not addressed in this study, may require further investigation and refinement of the weighing strategy.

6. Conclusions

This paper presents a SETSM-based multiple-pair DSM generation framework designed for the automated production of high-quality, large-scale, digital surface models (DSMs) using PlanetScope PS2 imagery. The proposed framework integrates (1) a novel optimized stereo pair selection strategy based on Weighted Stereo Pair Index (WSPI) to preferentially select well-defined stereo pairs and optimize computation loads, (2) an inter-

plane vertical coregistration technique that internally generates reference surfaces and effectively reduces vertical biases without relying on ground control points or external reference DSMs, and (3) a modified integrated weight function (IWHq) within the SETSM 3D KWHE algorithm. These integrated components effectively addressed key challenges associated with narrow convergence angles, image texture inconsistencies, surface noise, and vertical biases between stereo pairs in order to improve DSM quality and enable fully automated DSM generation from PlanetScope PS2 imagery. By suggesting the maximum and minimum number of stereo pairs specified for a computing system and SETSM framework, the optimized stereo pair selection step automatically identifies well-defined stereo pairs without systematic failure through sequential conditional filtering and the development of the WSPI, which incorporates geometric suitability, texture quality, mapping completeness and image-matching quality. The inter-plane vertical coregistration significantly improves the PSMDSM accuracy, achieving up to 43% reductions in RMSE, and increasing the proportion of grid cells within the '0 to 5 m' height difference range by up to 26%, compared to PSMDSMs generated without relative vertical coregistration and RPC bias correction. PSMDSMs produced with a reduced tile size of 5 km demonstrate accuracy comparable to those generated using absolute VC approaches because scaling effects and vertical biases arising from the expansion and merging of multiple DSMs are effectively minimized during the step of reference surface generation. The observed relationship between PSMDSM accuracy and terrain height range supports the model's performance predictability. However, tile inconsistencies in mosaicked PSMDSMs and the influence of surface height range and satellite geometry must be attentively recognized by users. Validation from five impact craters with varying environments and surface relief confirms the robustness and generalizability of the proposed framework. With the capability to reconstruct detailed terrain features at a 4 m spatial resolution and with reduced surface noise, including in persistently cloudy regions, the PSMDSM framework shows strong potential to provide the first global DSM at a spatial resolution of less than 10 m, provided that vertical bias mitigation is carefully implemented. The developed algorithms of optimized stereo pair selection, inter-plane vertical coregistration, and integrated weight function are broadly applicable to other DSM generation methodologies through appropriate modifications to accommodate differences in matching attributes and system architecture. Future work will focus on further advancing the coregistration step to reduce dependency on the attributes of the reference stereo pair and to better mitigate scale-dependent vertical errors. In addition, extensive validation with various terrain sites will be performed to enhance the applicability of the proposed methodology, including comparisons with high-quality DSMs derived from WorldView in-track stereo images. Other products of PlanetScope imagery such as Dove-R and SuperDove will be tested and analyzed in terms of DSM quality and viewing geometry.

Author Contributions: Conceptualization, M.-J.N.; methodology, M.-J.N.; software, M.-J.N.; validation, M.-J.N.; formal analysis, M.-J.N.; investigation, M.-J.N.; resources, M.-J.N. and I.M.H.; data curation, M.-J.N. and I.M.H.; writing—original draft preparation, M.-J.N.; writing—review and editing, I.M.H.; visualization, M.-J.N.; supervision, I.M.H.; project administration, I.M.H.; funding acquisition, M.-J.N. and I.M.H. All authors have read and agreed to the published version of the manuscript.

Funding: This research was funded by grants #80NSSC22K1093 and #80NSSC20K1422 from the U.S. National Aeronautics and Space Administration and #1559691 from the U.S. National Science Foundation Office of Polar Programs.

Data Availability Statement: PlaneScope PS2 and Maxar WorldView images were obtained from the Polar Geospatial Center as part of the EarthDEM project supported by the National Geospatial-

Intelligence Agency (NGA) and National Science Foundation Office of Polar Programs (NSF OPP A010607701).

Acknowledgments: The Polar Geospatial Center provided the satellite imagery.

Conflicts of Interest: The authors declare no conflicts of interest. The funders had no role in the design of the study; in the collection, analyses, or interpretation of data; in the writing of the manuscript; or in the decision to publish the results.

Abbreviations

The following abbreviations are used in this manuscript:

DSM	Digital Surface Model
GCP	Ground Control Point
TIN	Triangular Irregular Network
SETSM	Surface Extraction by TIN-Based Search-Space Minimization
WSPI	Weighted Stereo Pair Index
RPC	Rational Polynomial Coefficient
RMSE	Root Mean Square Error
GSD	Ground Sample Distance
SGM	Semi-Global Matching
SRTM	Shuttle Radar Topography Mission
AOI	Area Of Interest
MMP	Multiple-Pair Matching Procedure
KWHE	Kernel-Based Weighted Height Estimation
HPC	High Performance Computing
USGS	United States Geological Survey
EROS	Earth Resources Observation and Science
PS	PlanetScope
SP	Stereo Pair
AA	Asymmetry Angle
BEA	Bisector Elevation Angle
CA	Convergence Angle
PSMDSM	PlanetScope Multiple-Image-Derived DSM
API	Application Programming Interface
MP	Matching Point
VLL	Vertical-Line Locus
IP	Inter-Pair
NCC	Normalized Cross-Correlation
GNCC	Geometrically Corrected NCC
UNCC	Uncorrected NCC
VC	Vertical Coregistration
WLSA	Weighted Least Squares Adjustment
LSF	Local Surface Fitting
PSSDSM	PlanetScope Single-Pair DSM
LB	Lower Bound
UB	Upper Bound

References

1. Planet Analytic Imagery and Archive. Available online: https://www.planet.com/products/satellite-imagery-of-earth/ (accessed on 26 December 2025).
2. PlanetScope Technical Specification. Available online: https://docs.planet.com/data/imagery/planetscope/techspec/ (accessed on 16 February 2026).
3. Sarkar, S.; Sagan, V.; Bhadra, S.; Bhodes, K.; Pokharel, M.; Fritschi, F.B. Soybean seed composition prediction from standing crops using PlanetScope satellite imagery and machine learning. *ISPRS J. Photogram. Remote Sens.* **2024**, *204*, 257–274. [CrossRef]

4. Yao, Y.; Hu, C.; Cannizzaro, J.P.; Zhang, S.; Barnes, B.B.; Xie, Y.; Qi, L.; Armstrong, C.; Chen, Z. Detecting cyanobacterial blooms in the Caloosahatchee river and estuary using PlanetScope imagery and deep learning. *IEEE Trans. Geosci. Remote Sens.* **2024**, *62*, 4202513. [CrossRef]
5. Kluczek, M.; Aagajewski, B.; Zwijacz-Kozica, T. Mountain tree species mapping using Sentinel-2, Planetscope, and airborne Hyspex hyperspectral imagery. *Remote Sens.* **2023**, *15*, 844. [CrossRef]
6. Kimijima, S.; Nagai, M. High spatiotemporal flood monitoring associated with rapid lake shrinkage using Planet Smallsat and Sentinel-1 data. *Remote Sens.* **2023**, *15*, 1099. [CrossRef]
7. Duan, P.; Zhang, F.; Liu, C.; Tan, M.L.; Shi, J.; Wang, W.; Cai, Y.; Kung, H.-T.; Yang, S. High-resolution PlanetScope imagery and machine learning for estimating suspended particulate matter in the Ebinur lake, Xinjiang, China. *IEEE J. Select. Top. Appl. Earth Obs. Remote Sens.* **2023**, *16*, 1019–1032. [CrossRef]
8. John, A.; Cannistra, A.F.; Yang, K.; Tan, A.; Shean, D.; Lambers, J.H.R.; Cristea, M. High-resolution snow-covered area mapping in forested mountain ecosystems using PlanetScope imagery. *Remote Sens.* **2022**, *14*, 3409. [CrossRef]
9. Sagan, V.; Maimaitijiang, M.; Bhadra, S.; Maimaitiyiming, M.; Brown, D.R.; Sidike, P.; Fritschi, F.B. Field-scale crop yield prediction using multi-temporal WoldView-3 and PlanetScope satellite data and deep learning. *ISPRS J. Photogram. Remote Sens.* **2021**, *174*, 265–281. [CrossRef]
10. Ghuffar, S. DEM generation with multi satellite PlanetScope imagery. *Remote Sens.* **2018**, *10*, 1462. [CrossRef]
11. Hirschmuller, H. Stereo Processing by Semiglobal Matching and Mutual Information. *IEEE Trans. Pattern Anal. Mach. Int.* **2007**, *30*, 328–341. [CrossRef]
12. Aati, S.; Avouac, J.-P. Optimization of optical image geometric modeling, application to topography extraction and topographic change measurements using PlanetScope and SkySat imagery. *Remote Sens.* **2020**, *12*, 3418. [CrossRef]
13. d'Angelo, P.; Reinartz, P. Digital elevation models from stereo, video and multi-view imagery captured by small satellites. *Int. Arch. Photogramm. Remote Sens. Spat. Inf. Sci.* **2021**, *XLIII-B2-2021*, 77–82. [CrossRef]
14. Huang, D.; Tang, Y.; Qin, R. An evaluation of planetscope images for 3D reconstruction and change detection-Experimental validations with case studies. *GIScience Remote Sens.* **2022**, *59*, 744–761. [CrossRef]
15. Qin, R. Automated 3D Recovery from Very High Resolution Multi-view Satellite Images. In Proceedings of the ASPRS (IGTF) Annual Conference, Baltimore, MD, USA, 12–16 March 2017.
16. Noh, M.; Howat, I.M. Extending SETSM capability from stereo to multi-pair imagery. *Remote Sen.* **2025**, *17*, 3206. [CrossRef]
17. Noh, M.; Howat, I.M. Analysis of PlanetScope Dove digital surface model accuracy using geometrically simulated images. *Remote Sens.* **2023**, *15*, 3496. [CrossRef]
18. Jeong, J.; Kim, T. Analysis of Dual-Sensor Stereo Geometry and Its Positioning Accuracy. *Photogramm. Eng. Remote Sens.* **2014**, *80*, 653–661. [CrossRef]
19. Planet Inc. Application Programming Interfaces (APIs). Available online: https://docs.planet.com/develop/apis/ (accessed on 26 December 2025).
20. Noh, M.; Howat, I.M. Automatic relative RPC image model bias compensation through hierarchical image matching for improving DEM quality. *ISPRS J. Photogram. Remote Sens.* **2018**, *136*, 120–133. [CrossRef]
21. Nuth, C.; Kääb, A. Co-registration and bias corrections of satellite elevation data sets for quantifying glacier thickness change. *Cryosphere* **2011**, *5*, 271–290. [CrossRef]
22. Osinski, G.R.; Grieve, R.A.F.; Ferriere, L.; Losiak, A.; Pickersgill, A.E.; Cavosie, A.J.; Hibbard, S.M.; Hill, P.J.A.; Bermudez, J.J.; Marion, C.L.; et al. Impact Earth: A review of the terrestrial impact record. *Earth Sci. Rev.* **2022**, *232*, 104112. [CrossRef]
23. Rochette, P.; Alac, R.; Beck, P.; Brocard, G.; Cavosie, A.J.; Debaille, V.; Devouard, B.; Jourdan, F.; Mougel, B.; Mustard, F.; et al. Pantasma: Evidence for a Pleistocene circa 14 km diameter impact crater in Nicaragua. *Meteorit. Planet. Sci.* **2019**, *54*, 880–901. [CrossRef]
24. Rochette, P.; Beck, P.; Bizzarro, M.; Braucher, R.; Cornec, J.; Debaille, V.; Devouard, B.; Gattacceca, J.; Jourdan, F.; Moustard, F.; et al. Impact glasses from Belize represent tektites from the Pleistocene Pantasma impact crater in Nicaragua. *Commun. Earth Environ.* **2021**, *2*, 94. [CrossRef]
25. USGS EathExplorer. Available online: https://earthexplorer.usgs.gov/ (accessed on 26 December 2025).
26. Noh, M.; Howat, I.M. Automated coregistration of repeat digital elevation models for surface elevation change measurement using geometric constraints. *IEEE Tran. Geosci. Remote Sens.* **2014**, *52*, 2247–2260. [CrossRef]

Disclaimer/Publisher's Note: The statements, opinions and data contained in all publications are solely those of the individual author(s) and contributor(s) and not of MDPI and/or the editor(s). MDPI and/or the editor(s) disclaim responsibility for any injury to people or property resulting from any ideas, methods, instructions or products referred to in the content.